

# GPHR is a novel anion channel critical for acidification and functions of the Golgi apparatus

Yusuke Maeda<sup>1,2,3,9</sup>, Toru Ide<sup>4,5</sup>, Masato Koike<sup>6,8</sup>, Yasuo Uchiyama<sup>6,8</sup> and Taroh Kinoshita<sup>1,2,7</sup>

The organelles within secretory and endocytotic pathways in mammalian cells have acidified lumens, and regulation of their acidic pH is critical for the trafficking, processing and glycosylation of cargo proteins and lipids, as well as the morphological integrity of the organelles. How organelle lumen acidification is regulated, and how luminal pH elevation disturbs these fundamental cellular processes, is largely unknown. Here, we describe a novel molecule involved in Golgi acidification. First, mutant cells defective in Golgi acidification were established that exhibited delayed protein transport, impaired glycosylation and Golgi disorganization. Using expression cloning, a novel Golgi-resident multi-transmembrane protein, named Golgi pH regulator (GPHR), was identified as being responsible for the mutant cells. After reconstitution in planar lipid bilayers, GPHR exhibited a voltage-dependent anion-channel activity that may function in counterion conductance. Thus, GPHR modulates Golgi functions through regulation of acidification.

In mammalian cells, luminal acidification of organelles within secretory and endocytic pathways is critical for various cellular functions<sup>1</sup>. When the acidic luminal pH is alkalinized by weak bases, a proton ionophore or inhibitors of vacuolar H<sup>+</sup>-ATPase (V-ATPase), the trafficking, processing and glycosylation of cargo proteins and lipids are impaired<sup>2–6</sup>, some proteins become missorted<sup>5,7–9</sup> and the morphological integrity of the Golgi is compromised<sup>2,3,10</sup>. The mechanisms underlying these phenomena are not well understood because of insufficient knowledge at the molecular level and the absence of mutant cells defective in Golgi pH regulation<sup>11</sup>. Alterations of luminal pH have been implicated in congenital diseases<sup>1,12,13</sup> and cancer<sup>6,14</sup>, indicating that regulation of pH in intracellular organelles is a fundamental component of homeostasis<sup>1</sup>. It has been assumed that the acidic pH of organelles, including the Golgi, is regulated by a balance between the rates of intraluminal proton delivery by V-ATPase, counterion conductance and intrinsic proton leakage<sup>15–24</sup>. V-ATPase, a highly conserved proton pump, is thought to be the sole source of proton delivery and is known to be regulated by a number of different mechanisms<sup>25</sup>. Counterion conductance decreases the membrane potential formed by proton influx to allow V-ATPase to transfer more protons into the Golgi lumen<sup>16</sup>. Potassium (K<sup>+</sup>) and chloride (Cl<sup>-</sup>) are candidate counterions. Several chloride channels are expressed in intracellular organelles, including members of the voltage-dependent Cl<sup>-</sup> channel (ClC)<sup>26,27</sup>, Cl<sup>-</sup> intracellular channel<sup>28</sup>, mid-1-related chloride channel<sup>29</sup> and Golgi anion channel (GOLAC) families<sup>30,31</sup>. Some of these channels are implicated in

endosomal acidification<sup>18,32</sup>, but none have been proven to be involved in luminal acidification of the Golgi. Therefore, the significance of counterion channels for Golgi pH regulation remains unclear<sup>19–23</sup>. A third factor, intrinsic proton leakage, which is more active in the endoplasmic reticulum (ER) and less active in the *trans*-Golgi network (TGN), has been suggested to create a pH gradient along the secretory pathway<sup>19,23</sup>, but little is known about its molecular mechanism.

Here, we describe a newly established mutant cell line and identification of GPHR, which may be the first counterion channel shown to be critical for Golgi pH regulation.

## RESULTS

### Establishment and characterization of a mutant cell line with delayed protein transport

To establish mutant cells with defective protein transport the reporter molecule, VSVG<sup>ex</sup>-Flag-EGFP-GPI was used (Supplementary Information, Fig. S1). To establish the parental FF8 cell line, Chinese hamster ovary (CHO) cells expressing human CD59 and decay accelerating factor (DAF) were stably transfected with the reporter gene whose expression was driven by a doxycycline (Dox)-dependent inducible promoter. The reporter protein was induced by adding Dox at the non-permissive temperature of 40 °C, thereby causing accumulation of the reporter protein in the ER, which could then be released from the ER by shifting the culture temperature to 32 °C. Transport of the reporter protein to the plasma

<sup>1</sup>Research Institute for Microbial Diseases, Osaka University, Suita, Osaka 565–0871, Japan. <sup>2</sup>WPI Immunology Frontier Research Center, Osaka University, Suita, Osaka 565–0871, Japan. <sup>3</sup>PRESTO Japan Science and Technology Agency, Saitama 332–0012, Japan. <sup>4</sup>Laboratories for Nanobiology, Graduate School of Frontier Biosciences, Osaka University, Suita, Osaka 565–0871, Japan. <sup>5</sup>Molecular-Informational Life Science Research Group, RIKEN, Wako 351–0198, Japan. <sup>6</sup>Department of Cell Biology and Neurosciences, Graduate School of Medicine, Osaka University, Suita, Osaka 565–0871, Japan. <sup>7</sup>CREST, Japan Science and Technology Agency, Saitama 332–0012, Japan. <sup>8</sup>Current address: Department of Cell Biology and Neuroscience, Juntendo University School of Medicine, Tokyo 113–8421, Japan.  
<sup>9</sup>Correspondence should be addressed to Y.M. (e-mail: ymaeda@biken.osaka-u.ac.jp)

Received 11 July 2008; accepted 20 August 2008; published online 14 September 2008; DOI: 10.1038/ncb1773

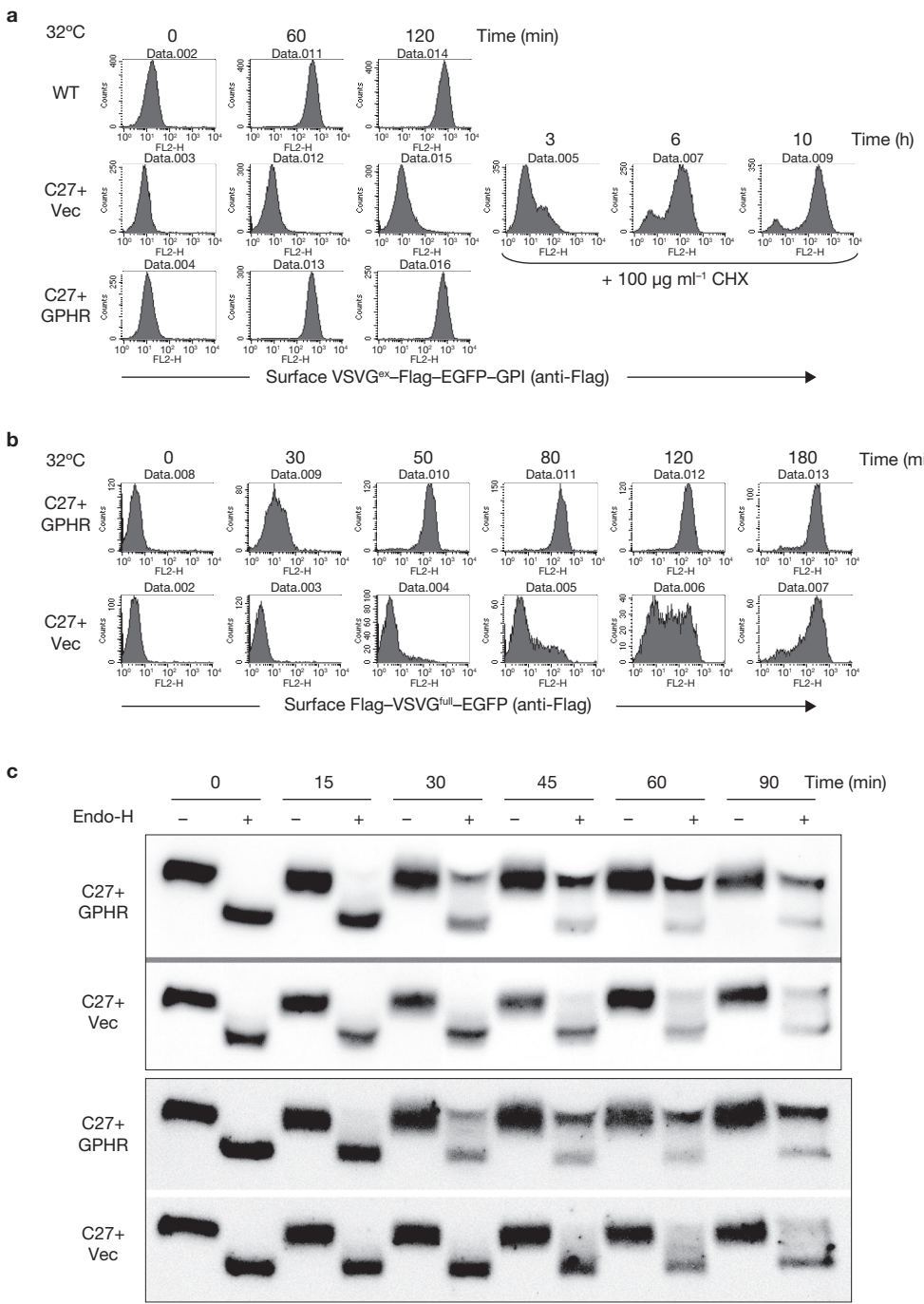


**Figure 1** Delayed transport of newly synthesized proteins in mutant cells. **(a, b)** Flow cytometric analyses of the surface expressions of reporter proteins at the indicated times after a temperature shift from 40 °C to 32 °C in transport assays. Parent FF8, mock vector-transfected mutant C27 (C27+Vec) and GPHR-transfected C27 (C27+GPHR) cells expressing VSVG<sup>ex</sup>-Flag-EGFP-GPI (**a**) and Flag-VSVG<sup>full</sup>-EGFP (**b**) were stained with an anti-Flag antibody. Cycloheximide (CHX; 100 µg ml<sup>-1</sup>) was included in the medium for

membrane was monitored by flow cytometric analysis of the surface expression of the Flag-tag at the indicated times after the temperature shift (Fig. 1a). FF8 cells were mutagenized with ethyl methanesulfonate and several rounds of similar transport assays were performed to sort out the mutant FF8 cells displaying delayed transport of the reporter protein.

cultures longer than 3 h. **(c)** Delayed protein transport in C27+Vec mutant cells. Non-tagged full-length temperature-sensitive VSVG protein expressed in C27+GPHR and C27+Vec cells at 40 °C for 24 h followed by incubation at 32 °C for the indicated times in the presence of 100 µg ml<sup>-1</sup> cycloheximide was treated with (+) or without (-) endoglycosidase-H (endo-H) and analysed by SDS-PAGE and western blotting with an anti-VSVG antibody. The results of two independent experiments are shown. WT, wild-type.

Mutant clone 27 (C27) cells were finally obtained. Mock-transfected C27 (C27+Vec) mutant cells showed much slower transport of the reporter protein than the parental FF8 cells (Fig. 1a). Another non-GPI-type reporter protein, Flag-VSVG<sup>full</sup>-EGFP (see Supplementary Information, Fig. S1), was also transported to the plasma membrane at a much slower

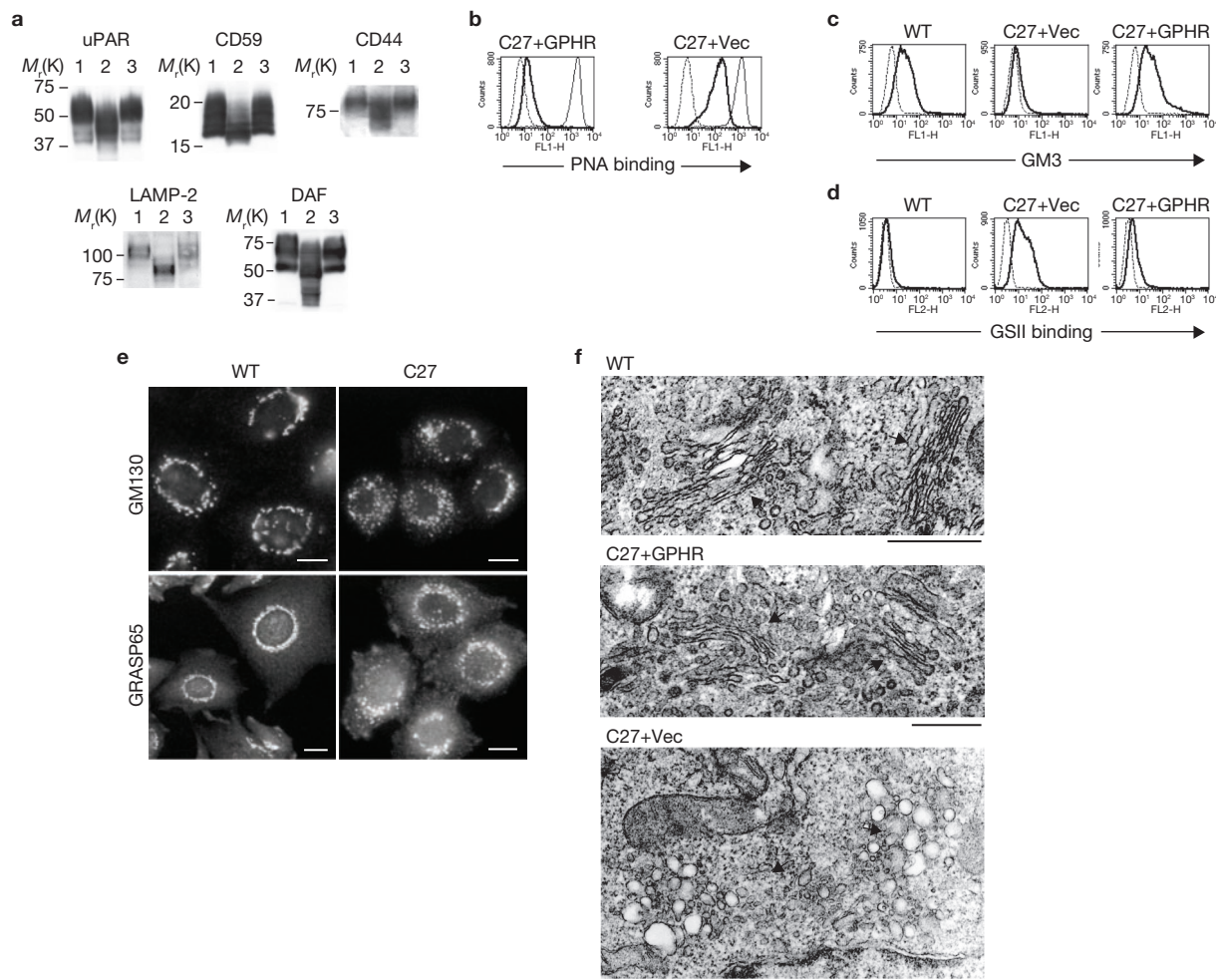


**Figure 2** Impaired glycosylation and Golgi disorganization in mutant cells. **(a)** SDS-PAGE and western-blot analysis of various glycoproteins expressed in wild-type (lane 1), C27 (lane 2) and C27+GPHR (lane 3) cells. uPAR, urokinase-type plasminogen activator receptor. **(b)** Aberrant O-glycan expression (bold lines) because of insufficient sialylation is revealed by increased staining with FITC-conjugated peanut agglutinin (PNA). Dotted lines, no staining (background); solid lines, staining of sialidase-treated cells. **(c)** Mutant C27+Vec cells have lower surface expression of the GM3 ganglioside than wild-type and C27+GPHR cells. Dotted lines, background staining. **(d)** Mutant C27+Vec cells express higher levels of

terminal non-reducing N-acetyl-D-glucosamine in immature glycoproteins than wild-type and C27+GPHR cells. Dotted lines, background staining. **(e)** Immunofluorescent staining of the Golgi marker proteins GM130 and GRASP65 in wild-type and C27 cells. The staining profiles of both proteins are more fragmented and dispersed in C27 cells than in wild-type cells. The scale bars represent 10 μm. **(f)** Electron micrographs showing that Golgi stacks are lost and the cisternae are swollen and vesiculated in C27+Vec cells (arrows in bottom panel), whereas stacked cisternae are present in wild-type and C27+GPHR cells (arrows in top and middle panels). The scale bars represent 0.5 μm.

rate in C27 cells than in FF8 cells (Fig. 1b). Importantly, C27+GPHR cells, which were established by stable transfection of the GPHR gene into C27 mutant cells, exhibited complete restoration of the delayed transport of both reporter proteins (Fig. 1a, b). C27+Vec mutant cells showed a distinct delay in the appearance of endoglycosidase-H-resistant VSVG (Fig. 1c). Thus, defective transport from the ER to the plasma membrane was common for both GPI-anchored and transmembrane cargos. The transport delay was more prominent for the GPI-anchored reporter protein, probably due to the construction or nature of this reporter (see Supplementary Information).

Two other abnormal phenotypes were observed: impaired glycosylation and Golgi-apparatus disorganization. All the glycosylated proteins analysed had smaller relative molecular masses in C27 cells than in FF8 cells (Fig. 2a). CD59 has only one N-glycosylation site. N-glycanase treatment of CD59 in wild-type and mutant cells yielded proteins of

the same relative molecular mass (see Supplementary Information, Fig. S2a), indicating that N-glycosylation was affected. DAF has one N-glycan and multiple O-glycans. The decrease in size of an intense band with a relative molecular mass of approximately 65,000 ( $M_r$ , 65K) to approximately 50K in C27 cells (Fig. 2a) was much larger than the sole defect of N-glycosylation and very close to that of sialidase-treated DAF in wild-type cells (see Supplementary Information, Fig. S2b), indicating that O-glycosylation was also affected. In fact, peanut agglutinin (PNA), a lectin that recognizes a truncated O-glycan lacking sialyl residues called T-antigen, stained C27 cells approximately tenfold more strongly than wild-type cells (Fig. 2b). In addition to protein N- and O-glycosylation, lipid glycosylation was impaired, as determined by the observation that GM3 levels (the sole ganglioside expressed in CHO cells) were significantly decreased (Fig. 2c). As these three impaired glycosylation processes could be explained by a single defect in sialylation, we examined

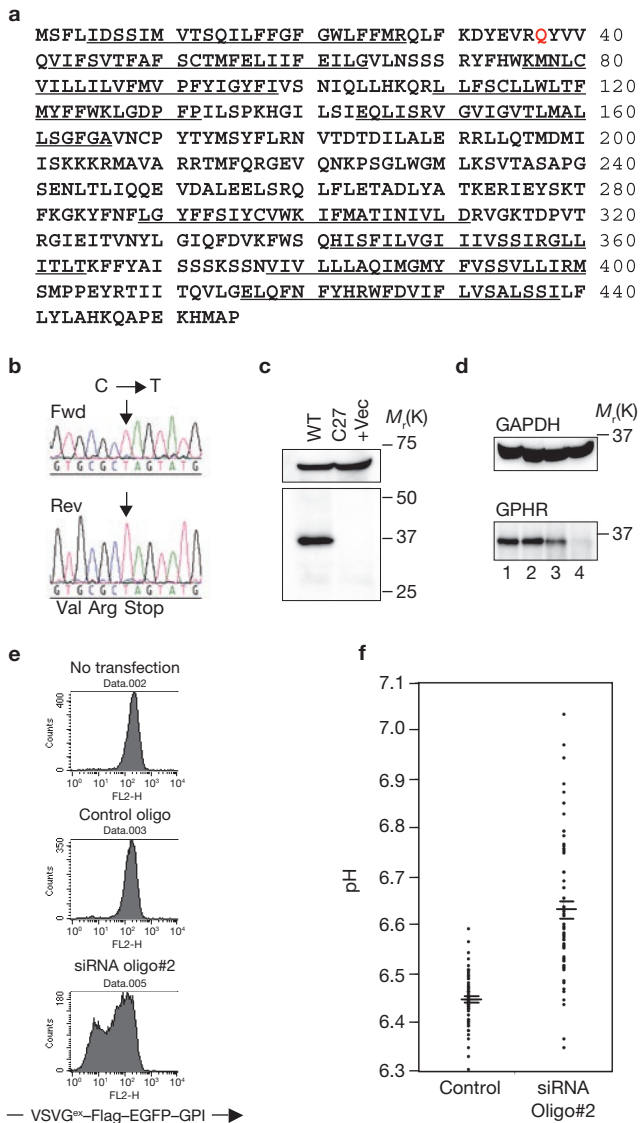


**Figure 3** GPHR is responsible for the defective phenotypes in C27 cells. (a) Amino acid sequence of hamster GPHR. Transmembrane regions indicated by SOSUI program are underlined. The red Q is mutated to a stop codon in C27 cells as shown in b. (b) Sequencing of GPHR from C27 cells reveals the presence of a nonsense mutation (CAG→TAG) in the codon for Glu 37 (arrows). The real waves of sequencing in the sense (Fwd) and antisense (Rev) directions are shown. (c) The amounts of endogenous GPHR were assessed by immunoprecipitation followed by western blot analysis of GPHR (lower panel). Similar amounts of ribophorin II were detected in the whole cell lysates used for the immunoprecipitation (upper panel). (d) The expression levels of GPHR and control GAPDH were analysed in parent FF8 cells without transfection (lane 1) and FF8 cells transfected with negative control (lane 2), GPHR-specific siRNA oligo #1 (lane 3) and GPHR-specific siRNA oligo #2 (lane 4) for three days. (e) Flow cytometric analyses of reporter protein VSVG<sup>ex</sup>-Flag-EGFP-GPI transport to the cell surface at 1 h after a temperature shift from 40 °C to 32 °C in parent FF8 cells without transfection and FF8 cells transfected with negative control and GPHR-specific siRNA oligo#2 for five days. (f) Measurement of the luminal pH of the Golgi in FF8 wild-type cells expressing GnT1-pHluorin that were transfected with negative control and GPHR-specific siRNA oligo#2. The fluorescent intensities of GnT1-pHluorin in 65 fields taken by confocal microscopy were analysed to measure pHs (see Fig. 4). The calculated pHs ( $6.45 \pm 0.0064$ ; mean ± s.e.m.) for control and  $6.64 \pm 0.018$  for GPHR-specific siRNA oligo#2 transfected cells differed significantly ( $n = 65$ ; Welch's *t*-test,  $P < 0.0001$ ). The large and small bars indicate the mean and s.e.m., respectively.

whether other glycosylation steps were also affected. GS-II lectin binds to terminal non-reducing N-acetyl-D-glucosaminyl residues of glycoproteins, which are only disclosed after removal of the galactose residue in the N-glycan chain. C27 mutant cells showed stronger staining with GS-II than wild-type cells (Fig. 2d). Therefore, we concluded that multiple glycosylation steps involved in the N- and O-glycosylation and glycosphingolipid production processes were impaired. Immunofluorescent staining of several Golgi proteins (such as GM130, GRASP65 and GS28) revealed a more fragmented and dispersed Golgi structure in C27 cells (Fig. 2e and data not shown), indicating a third defective phenotype. Electron microscopy revealed severe disorganization of the Golgi structure with loss of stacks, in addition to swelling and vesiculation of cisternae in C27 cells (Fig. 2f). Despite these three prominent phenotypes, C27+Vec and C27+GPHR cells grew at comparable rates, although adhesion and spreading on the plate seemed somewhat slower in C27+Vec cells. Both impaired glycosylation and Golgi-apparatus disorganization (Fig. 2a-d and f) were corrected by stable transfection of the GPHR gene in C27 mutant cells, indicating that all the defective phenotypes of C27 mutant cells were caused by a defect in GPHR.

#### Identification of GPHR

The gene responsible for the defects in C27 cells was identified by expression cloning based on restored reporter protein transport. The identified gene was previously recorded as G protein-coupled receptor 89 (GPR89; gene accession number, NM\_016334 for *Homo sapiens*) in the HUGO gene nomenclature system with no proven functions. As no structural similarities with other G protein-coupled receptors were observed and its role in pH regulation was clarified, we named the gene Golgi pH regulator (GPHR). GPHR protein was predicted to have multiple transmembrane regions by the SOSUI program, but had no known conserved domains. GPHR was well conserved among vertebrates, insects and plants (see Supplementary Information, Fig. S3), and seemed to be ubiquitously expressed (see Supplementary Information, Fig. S4).

To confirm that GPHR was the primary defect in C27 cells, the hamster GPHR gene was identified in CHO cells (gene accession number, AB362891; Fig. 3a), mRNA was analysed in the C27 mutant cells and a nonsense mutation in the codon for glutamine-37 was observed that would result in a small truncated peptide of 36 amino acids. Mutant transcripts were detected by RT-PCR whereas normal transcripts were not (Fig. 3b) — presumably because of the functional hemizygosity known to occur in many genes in CHO cells. Consistent with the RT-PCR data, no GPHR protein was detected in C27 mutant cells (Fig. 3c). RNA interference (RNAi) was used to verify that defective GPHR was sufficient to cause the mutant phenotypes. GPHR-specific short interference RNA (siRNA) oligonucleotide #2, but not siRNA oligonucleotide #1 or a control oligonucleotide, efficiently decreased GPHR protein expression in FF8 wild-type cells (Fig. 3d) and caused a significant delay in the transport of the reporter protein to the cell surface (Fig. 3e), although the phenotype was much weaker than that of the mutant cells (Fig. 1a). The luminal pH of the Golgi was then measured in FF8 wild-type cells subjected to siRNA as the primary defect in mutant cells was an elevation of the pH. The pH was elevated significantly in siRNA #2-treated cells (mean ± s.e.m. of pH:  $6.64 \pm 0.018$ ) compared with control oligonucleotide-treated cells ( $6.45 \pm 0.0064$ ; Fig. 3f). Consistent with the weaker defective phenotypes, the elevation was not as big in C27+Vec mutant cells (Fig. 4d). Thus, the defect in GPHR was concluded to be the primary cause for the phenotypes in mutant cells.

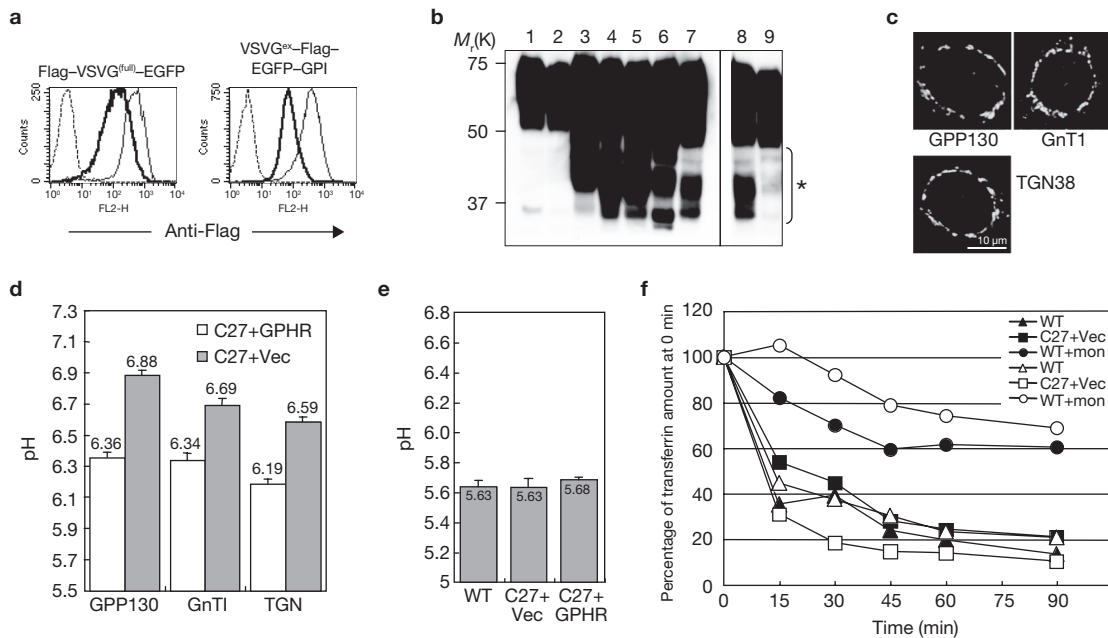


**Figure 4** Impaired luminal acidification of the Golgi is the primary defect in C27 cells. **(a)** Transport assays with two reporter proteins in the presence (bold lines) or absence (solid lines) of 10 μM monensin added to the culture medium when the culture was shifted from 40 °C to 32 °C. After 1 h, the surface expression of the reporter proteins were examined by FACS. Dotted lines, background staining without anti-Flag antibody. **(b)** Effects of various compounds on the glycosylation of DAF. The relative molecular masses of DAF in C27+GPHR (lanes 1–6) and C27+Vec (lanes 7–9) cells incubated with various reagents for 24 h were analysed by western blotting. The smaller-sized bands marked by the asterisk indicate immature glycosylation. Lanes 1, 7 and 8: no reagents; lanes 2 and 9: culture medium adjusted to pH 6.2; lane 3: 50 mM NH<sub>4</sub>Cl; lane 4: 10 μM monensin; lane 5: 0.4 μM baflomycin A; lane 6: 0.4 mM chloroquine. **(c)** Golgi–TGN localizations of three Golgi pH-sensor proteins: GPP130–pHluorin, GnT1–pHluorin and pHluorin–TGN38. The scale bar represents 10 μm. **(d)** Measurement of the luminal pH of the Golgi–TGN. The calculated pHs for C27+GPHR and C27+Vec cells differ significantly for all three Golgi pH-sensor proteins ( $n = 117$ –220; Student's *t*-test,  $P < 0.0001$  for each of the three proteins). The bars indicate the s.e.m. **(e)** Measurement of lysosomal pH in wild-type, C27+Vec and C27+GPHR cells. None of the pH differences for three cell types differ significantly in three independent experiments ( $n = 3$ ; Student's *t*-test: C27+Vec versus C27+GPHR,  $P = 0.188$ ; WT versus C27+GPHR,  $P = 0.207$ ; C27+Vec versus WT,  $P = 0.948$ ). The bars indicate the s.d. **(f)** Kinetics of transferrin recycling to the plasma membrane. The amounts of transferrin retained in the cells at the indicated times after exchange of transferrin-loading medium for serum-free medium were evaluated. The amount of transferrin at 0 min was set as 100% for each cell line. As a control, 5 μM monensin was added to the serum-free medium (WT+mon). Two independent experiments were performed, as indicated by open and closed symbols.

### Impaired acidification of the Golgi is the primary defect

As the three defective phenotypes of C27 mutant cells were similar to phenotypes caused by compounds that raise the Golgi pH (refs 2–10), we speculated that acidification of the Golgi might be disturbed. Monensin, an ionophore functioning as Na<sup>+</sup>/H<sup>+</sup> antiporter, caused delayed transport of both the GPI- and non-GPI-anchored transmembrane reporter proteins in our transport assay (Fig. 4a). Compounds that raise the Golgi pH caused impaired glycosylation of DAF, similar to observations in C27 cells (Fig. 4b) and culturing C27 cells in acidic medium normalized the glycosylation of DAF (Fig. 4b). The pH of the Golgi lumen was then directly assessed by constructing three chimeric indicator proteins (a pH-dependent ratiometric GFP called pHluorin<sup>33</sup> fused with the Golgi-targeting signal from GPP130 for the *cis*-Golgi; N-acetylglucosaminyltransferase I, GnT1, for the medial–*trans* Golgi; and TGN38 for the TGN) and stably integrating them into C27+Vec and C27+GPHR cells. All the chimeric indicator proteins were expressed in the Golgi and TGN (Fig. 4c). The results indicated that the luminal pHs were elevated by 0.35–0.52 in mutant cells (Fig. 4d). The pH values obtained for GPHR-restored C27 cells were consistent with those reported for normal cells<sup>6,21–23,34,35</sup>. The lysosomal pH in C27+Vec cells was approximately 5.6, which was slightly higher than a previously reported value<sup>36,37</sup>, and there were no significant differences

represents 10 μm. **(d)** Measurement of the luminal pH of the Golgi–TGN. The calculated pHs for C27+GPHR and C27+Vec cells differ significantly for all three Golgi pH-sensor proteins ( $n = 117$ –220; Student's *t*-test,  $P < 0.0001$  for each of the three proteins). The bars indicate the s.e.m. **(e)** Measurement of lysosomal pH in wild-type, C27+Vec and C27+GPHR cells. None of the pH differences for three cell types differ significantly in three independent experiments ( $n = 3$ ; Student's *t*-test: C27+Vec versus C27+GPHR,  $P = 0.188$ ; WT versus C27+GPHR,  $P = 0.207$ ; C27+Vec versus WT,  $P = 0.948$ ). The bars indicate the s.d. **(f)** Kinetics of transferrin recycling to the plasma membrane. The amounts of transferrin retained in the cells at the indicated times after exchange of transferrin-loading medium for serum-free medium were evaluated. The amount of transferrin at 0 min was set as 100% for each cell line. As a control, 5 μM monensin was added to the serum-free medium (WT+mon). Two independent experiments were performed, as indicated by open and closed symbols.

between FF8, C27+Vec and C27+GPHR cells (Fig. 4e). To evaluate the pH in early-recycling endosomes the recycling kinetics of internalized transferrin (Tf) to the culture medium was evaluated as elevated pH in early-recycling endosomes was known to delay these kinetics<sup>4,38</sup>. No differences were observed in the recycling kinetics of Tf or the kinetics of its internalization (data not shown) between FF8 and C27+Vec cells, whereas FF8 cells incubated with monensin showed significantly delayed Tf recycling (Fig. 4f). Thus, the alkalinization in mutant cells was seemingly specific to the Golgi and TGN.

### GPHR is mainly localized in the Golgi

We examined whether GPHR is localized at the Golgi–TGN. As the level of endogenous GPHR was below the detectable limits of immunofluorescence microscopy, GPHR fused with three HA-tags at the carboxy-terminus (GPHR-3HA) was prepared, its ability to restore the mutant phenotype of C27 cells was confirmed (see Supplementary Information, Fig. S5) and the expressed protein was visualized with an anti-HA antibody. GPHR-3HA was detected in the perinuclear area and colocalized well with GM130, but not with lysosomal Lamp2, early endosomal EEA1 (Fig. 5a) or endocytosed Tf and Tf receptor (see Supplementary Information, Fig. S6). In some cells, weak reticular (but obscure) staining of GPHR-3HA was observed in the cytosolic area,

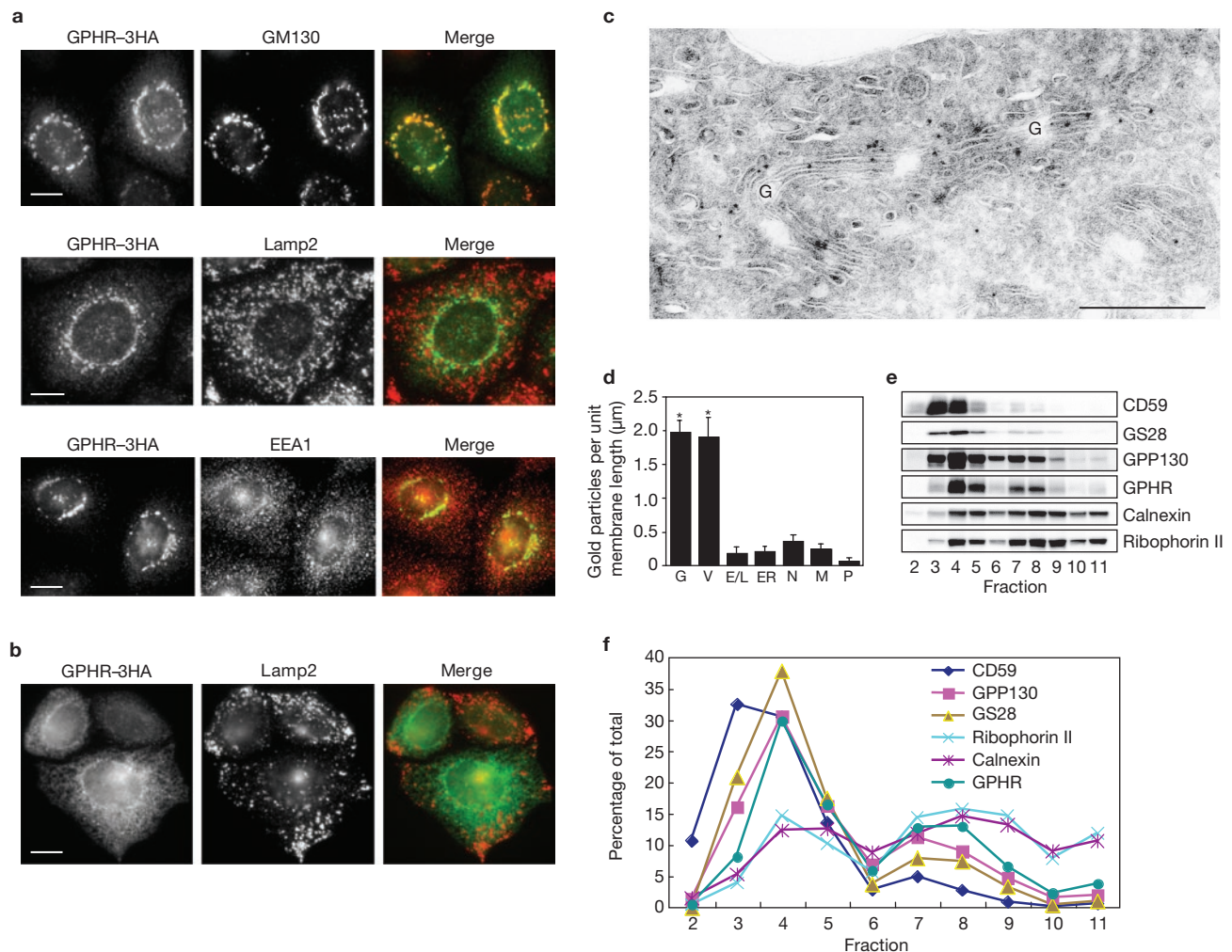


**Figure 5** GPHR is mainly localized at the Golgi. **(a, b)** Localization of GPHR-3HA protein. GPHR-3HA plus GM130, Lamp2 and EEA1 were stained in C27 cells stably expressing functional GPHR-3HA (C27+GPHR-3HA; **a**). GPHR-3HA and Lamp2 were stained in C27+GPHR-3HA cells at 30 min after treatment with 5  $\mu\text{g ml}^{-1}$  BFA (**b**). **(c)** Electron micrograph of an ultrathin cryosection of a C27+GPHR-3HA cell stained with an anti-HA antibody (10 nm colloidal gold particles). GPHR-3HA is enriched in the Golgi cisternae (G). Gold particles are also detected in vesicles around the Golgi. **(d)** The labelling densities in various intracellular membrane structures were quantified in electron micrographs similar to that shown in **c**. G, Golgi apparatus ( $n = 32$ ); V, peri-Golgi vesicles ( $n = 33$ ); E/L, endosome or lysosome ( $n = 20$ ); ER,

endoplasmic reticulum ( $n = 27$ ); N, outer nuclear membrane ( $n = 20$ ); M, outer mitochondrial membrane ( $n = 26$ ); P, plasma membrane ( $n = 31$ ). The data represent the means of 33 different cells. The bars indicate the s.e.m. The asterisks indicate  $P < 0.0001$  for Golgi apparatus or peri-Golgi vesicles versus others based on one-way ANOVA followed by Tukey Kramer *post hoc* test. **(e, f)** Subcellular fractionation of endogenous GPHR. Endogenous GPHR was immunoprecipitated from each subcellular fraction and analysed by immunoblotting (**e**). Other organelle marker proteins were detected in aliquots of the different subcellular fractions. The band intensities in **e** were quantified using a CCD luminescent image analyser and the percentages relative to the total of all fractions are shown (**f**). The scale bars represent 10  $\mu\text{m}$  in **a** and **b**, and 0.5  $\mu\text{m}$  in **c**.

which may indicate the ER. Treatment with brefeldin A (BFA) rendered the localization of GPHR-3HA similar to ER staining, which was quite different from that of BFA-treated lysosomes (Fig. 5b). The localization of GPHR-3HA was also examined by immunoelectron microscopy using ultrathin cryosections. GPHR-3HA was enriched in the Golgi cisternae and vesicles around the Golgi (Fig. 5c). The origin of the peri-Golgi vesicles was unclear and could be part of the Golgi, but immunogold labelling was rarely observed in lysosomes or multivesicular bodies (Fig. 5c, d). Subcellular fractionation was performed by sucrose density gradient ultracentrifugation to analyse the localization of endogenous GPHR. The distribution of endogenous GPHR coincided with the Golgi markers GPP130 and GS28, rather than with markers

for the plasma membrane (CD59) and ER (calnexin and ribophorin II; Fig. 5e, f). Taken together with the Golgi localization of GPHR-3HA, these results indicate that the majority of endogenous GPHR is localized in the Golgi.

#### GPHR is a novel anion channel

It is assumed that the acidic pH of the Golgi is regulated by a balance between the rates of intraluminal proton delivery, counterion conductance and intrinsic proton leakage. We speculated that multiple membrane-spanning GPHR may function as a counterion channel because GPHR was localized at the Golgi and loss of its function caused elevation of the Golgi pH. Therefore, we examined whether

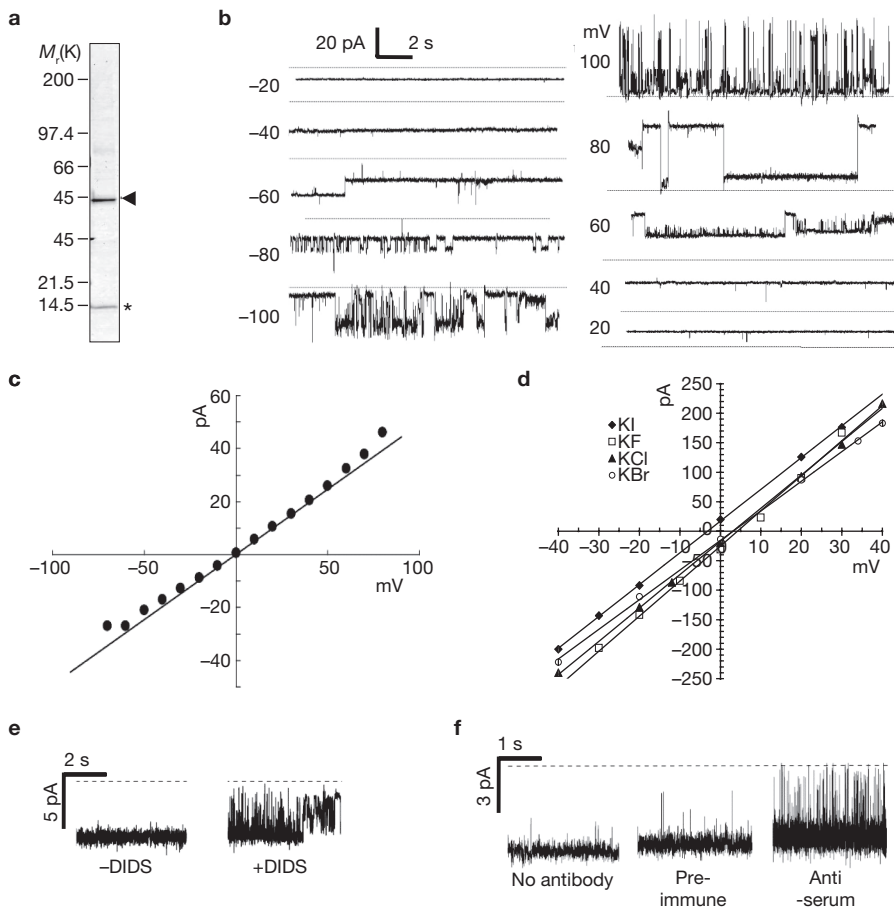


**Figure 6** GPHR is an anion channel. **(a)** Silver staining of purified GPHR–FHAT protein. GPHR–FHAT produced in Sf9 cells was sequentially purified using affinity columns against the tandem tags and the purity was assessed by silver staining. The band marked with an asterisk was confirmed to be degraded GPHR–FHAT by western blotting. **(b, c)** Channel conductance states in symmetrical 150 mM KCl solution. The current across the membrane was recorded at the indicated holding membrane potentials between the upper and lower solutions containing 150 mM KCl and 10 mM HEPES (pH 7.2). The current fluctuations of single GPHR–FHAT proteins indicate voltage dependence (**b**). The amplitudes of the single channel currents were plotted against the membrane potentials. A representative current–voltage (*I*–*V*) relationship of single-channel events is shown in **c**. **(d)** Channel conductance states in asymmetrical 210 mM KCl/150 mM Kx (x: anion) solution. The macroscopic currents across the membrane were

plotted against the membrane potentials as described in **c**. Relative anion permeabilities ( $P_x/P_{Cl^-}$ ) were measured by a shift of the reversal potential on replacement of  $Cl^-$  in the *trans* chamber with the various anions indicated. **(e)** Inhibition of the channel current with DIDS. DIDS (1 mM) was added to the upper chamber and the current amplitudes at a membrane potential of -10 mV were recorded before (-DIDS) and for several minutes after (+DIDS) the addition of DIDS. Upper horizontal lines, zero current. **(f)** Effects of an anti-GPHR serum on the channel activity. After reconstitution of a single anion channel into a lipid bilayer, preimmune or anti-GPHR rabbit serum was added to the upper compartment at 1:50 of the volume of the chamber. The current amplitudes at a membrane potential of -10 mV were recorded before (no antibody) and for several minutes after the addition of pre-immune (pre-immune) or anti-GPHR (anti-serum) serum. Upper horizontal line, zero current.

GPHR forms a channel. Attempts to express GPHR on the cell surface for patch-clamp analyses failed because GPHR did not localize to the plasma membrane in an overexpression system. An *in vitro* reconstitution of recombinant GPHR in an artificial lipid bilayer was then constructed. GPHR–FHAT (GPHR fused with Flag–HAT tandem tags at the C-terminus) was prepared, verified to be functional (see Supplementary Information, Fig. S5) and expressed in Sf9 insect cells. The recombinant GPHR–FHAT was purified to homogeneity by two sequential purification steps (Fig. 6a) and integrated into a planar lipid bilayer. GPHR–FHAT exhibited a typical single channel current with voltage-dependent fluctuations. The gating behaviour of this channel was complicated as it had at least four, and most likely five or six, subconductance states (Figs 6b and 7c). The channel was almost always in the open state when the absolute value of the membrane potential

was less than 30 mV, but tended to transit into subconductance states at larger potentials, indicating voltage dependence (Fig. 6b). The average conductance of the single channel was calculated to be  $400 \pm 99$  pS (mean  $\pm$  s.d.,  $n = 16$ ) from *I*–*V* curve (Fig. 6c). The voltage dependence, as well as the single-channel conductance, showed no significant changes in the presence of buffers ranging in pH from 5.3–7.4 (data not shown). From the reversal potential in asymmetrical KCl solution (300 mM/150 mM), the channel was determined to be more permeable to  $Cl^-$  than  $K^+$ , with a  $P_{Cl^-}/P_K$  permeability ratio of  $2.8 \pm 1.3$  (mean  $\pm$  s.d.,  $n = 5$ ), indicating that GPHR functions as an anion channel. As more than 90% of the single-channel activities observed in this system were those of anion channels, and because multiple-channel states also showed anion channel activities, the single-channel traces shown here were representative of the highly purified protein preparation.

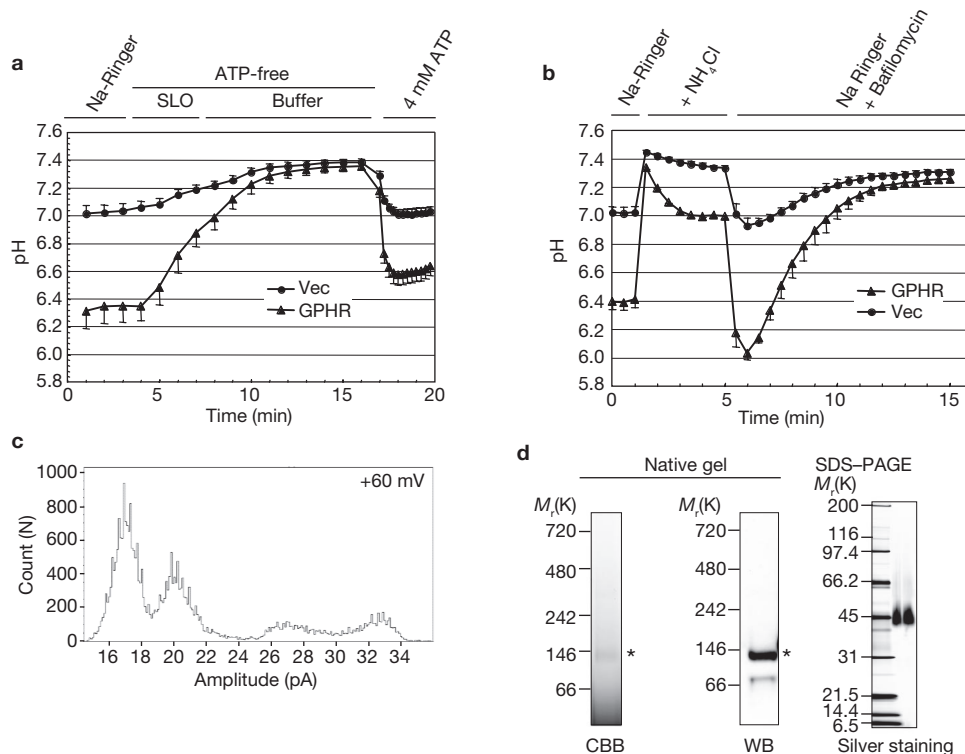


**Figure 7** Trimeric GPHR channel helps V-ATPase to acidify the Golgi lumen. **(a)** *In vitro* reconstitution of Golgi acidification in semi-intact cells permeabilized by streptolysin-O (SLO). C27+GPHR ( $n = 7$  independent experiments) and C27+Vec ( $n = 8$ ) cells expressing GnTI-pHluorin were sequentially incubated in permeabilization buffer containing  $0.5 \mu\text{g ml}^{-1}$  SLO for 5 min and permeabilization buffer alone for 8 min to deplete intracellular ATP. Next, 4 mM ATP was added back to the buffer to restore V-ATPase activity. In each experiment, several cells were analysed by the MetaMorph software to calculate the pH. The error bars indicate the s.e.m. **(b)** Estimation of the Golgi buffer capacities by the addition of NH<sub>4</sub>Cl. C27+GPHR ( $n = 4$ ) and C27+Vec ( $n = 6$ ) cells expressing GnTI-pHluorin were loaded with 30 mM NH<sub>4</sub>Cl. The buffer was then replaced with

Na-Ringer buffer supplemented with 1  $\mu\text{M}$  bafilomycin. The pH was monitored as described in **a**. The error bars indicate the s.e.m. **(c)** Amplitude histogram generated at a holding potential of +60 mV in symmetrical 150 mM KCl solution as shown in Fig. 6b. **(d)** Trimeric GPHR complex detection. C27 mutant cells expressing GPHR-FHAT were solubilized with 1% digitonin-containing buffer and GPHR-FHAT complexes were purified. The complexes were separated by blue-native PAGE (left) and analysed by western blotting with an antibody against the FLAG-tag (middle panel). The proteins marked with an asterisk, which was stained with Coomassie Brilliant Blue in the blue-native PAGE and confirmed to be a major complex including GPHR-FHAT by western blotting (middle), was excised and separated by SDS-PAGE. The proteins in the gel were visualized by silver staining.

To investigate the ionic selectivity of GPHR, the relative anion permeabilities ( $P_x/P_{Cl^-}$  where x is an anion) were measured (Fig. 6d). The halide anion permeability sequence was I<sup>-</sup> (1.5) > Cl<sup>-</sup> (1.0) = Br<sup>-</sup> (1.0) > F<sup>-</sup> (0.9) relative to Cl<sup>-</sup>. Methanesulfonate was impermeant (data not shown). Consistent with the nature of an anion channel, the channel was inhibited by 4,4'-diisothiocyanostilbene-2,2'-disulfonic acid (DIDS; Fig. 6e). After adding DIDS, the current amplitude began to flicker, shifted to subconductance states and eventually became almost completely blocked (see Supplementary Information, Fig. S7a). The slow response was most probably due to our inability to stir the solution vigorously. To verify that this anion channel behaviour was derived from GPHR protein and not from contaminating proteins, preimmune or anti-GPHR rabbit serum was added to the lipid bilayer system (Fig. 6f). There was no significant change in the current amplitude following the addition of preimmune serum, whereas the channel current amplitude began to flicker just after the addition of a 1:50 volume of anti-GPHR serum to the upper compartment. Although the single-channel current was not completely inhibited to the basal level, it rapidly made the transition to multiple subconductance states (Fig. 6f and see Supplementary Information, Fig. S7b, c), indicating that the anion channel behaviour did indeed arise from the function of GPHR.

The function of GPHR was further verified using a system of semi-intact cells permeabilized with streptolysin-O (SLO)<sup>24</sup>, in which V-ATPase-ATP-mediated Golgi acidification was inhibited or reconstituted by rapid and thorough substitution of the buffer composition. In both C27+GPHR and C27+Vec cells stably expressing GnTI-pHluorin, alkalinization of the Golgi pH to similar values (~7.4) was observed on permeabilization and depletion of ATP by SLO (Fig. 7a). The elevated pHs in both cell lines were rapidly decreased after reintroduction of exogenous ATP to almost the starting pH of each cell line (Fig. 7a), indicating that V-ATPase in C27+Vec cells was functional. This finding was strengthened by the observation that the Golgi pH in non-permeabilized mutant cells, as well as in wild-type cells, was more alkalinized than the starting pH by treatment with the V-ATPase inhibitor bafilomycin (Fig. 7b). As the elevated pH caused by depletion of ATP in C27+Vec cells was not decreased to a similar pH value observed in C27+GPHR after reintroduction of ATP (Fig. 7a), the GPHR defect impaired the Golgi acidification potential in the presence of functional V-ATPase. The elevation rate of Golgi pH ( $\Delta\text{pH min}^{-1}$ ) on inhibition of V-ATPase function by either ATP depletion (Fig. 7a) or addition of bafilomycin (Fig. 7b) was slower in C27+Vec cells than in C27+GPHR cells, even when compared in the same pH range of 7.0–7.2. To understand the

difference, the Golgi-compartment buffer capacities were calculated from the magnitudes of the pH increases in response to a pulse of 30 mM NH<sub>4</sub>Cl (Fig. 7b). The buffer capacities were  $29.5 \pm 0.8$  mM pH<sup>-1</sup> (mean  $\pm$  s.e.m.,  $n = 4$ ) in C27+GPHR cells, which was similar to a previously observed value<sup>35</sup>, and  $51.2 \pm 2.4$  mM pH<sup>-1</sup> ( $n = 6$ ) in C27+Vec cells. Thus, the difference of rates in the elevation of Golgi pH could arise from the differing buffer capacities of the cells and/or retardation of the conductive proton leakage by an intraluminal negative potential because of the defect in GPHR, which may function as a major counterion channel<sup>21</sup>. Finally, as ion channels that harbour multiconductance states are sometimes homo-oligomers<sup>39</sup> and as GPHR had multiple subconductance states (Figs 6b and 7c), we investigated whether the GPHR channel was composed of oligomeric proteins. After blue-native gel electrophoresis in the first dimension, the purified GPHR-FHAT complexes resulted in only a single band corresponding to a relative molecular mass of 130–140K (Fig. 7d). Western-blot analysis confirmed that this was the major complex containing GPHR-FHAT. A minor complex was detected at approximately 84K, but a band corresponding to single GPHR molecules was not observed. After SDS-PAGE in the second dimension, GPHR-FHAT was the only protein visualized by silver staining in the major band excised from the blue-native gel, indicating that the GPHR channel was composed of trimeric GPHR, consistent with the presence of multiple substates.

## DISCUSSION

There are several reports supporting a significant contribution of counterion conductance to Golgi acidification<sup>20,24</sup>, whereas other recent studies and models have indicated a smaller significance of counterion conductance for the maintenance of Golgi pH compared to intrinsic proton leakage<sup>19,21–23</sup>. We established mutant cells with an elevated Golgi pH and identified GPHR as the gene responsible for this defect. As the elevated pH in the mutant cells caused impaired trafficking and glycosylation of cargo proteins and lipids, as well as disrupted morphological integrity of the Golgi, GPHR is crucial for facilitating sufficient luminal acidification for normal Golgi functions. The GPHR gene encodes a Golgi-resident anion channel, suggesting that the function of GPHR is counterion conductance and that the anion channel is essential for physiological acidification. Currently, we cannot completely exclude the possibility that GPHR is involved in other processes — such as regulation of the function or localization of the Golgi pool of V-ATPase.

In mammalian cells, five members of CLC family are expressed in the endocytotic-lysosomal pathway<sup>26,27,40,41</sup>. Each organelle along the endocytotic-lysosomal pathway has a particular pH and it is speculated that each pH is regulated by the CLC members that are individually localized at appropriate organelles, which may be one of the reasons for the existence of so many family members. Nevertheless, the presence of CLC members in the Golgi has not been observed, which may explain the requirement for GPHR at the Golgi. GPHR is mainly expressed in the Golgi and TGN, but rarely in lysosomes and endosomes. Consistent with this localization, lysosomal pH and endosomal function were not disturbed in GPHR-mutant cells, indicating that GPHR specifically functions in the Golgi.

GOLAC-2, which has not been identified at the molecular level, was characterized as an anion channel existing in highly purified Golgi membranes using a planar lipid bilayer system<sup>31</sup>. Interestingly, there are several similarities between GPHR and GOLAC-2. GOLAC-2 has

a large anion conductance (325 pS), multiple (five or six) conductance states, relative insensitivity to changes in pH within the physiological range, a similar halide anion permeability sequence that corresponds to Eisenman sequence I (ref. 42) and voltage-dependent substrate occupancy. Although GPHR exhibited weaker selectivity for Cl<sup>-</sup> anions versus K<sup>+</sup> cations ( $P_{Cl^-}/P_K = 2.8$ ) than GOLAC-2 ( $P_{Cl^-}/P_K = 6.1$ ) and some of the values described above differ somewhat from those of the GPHR channel, these differences may arise from the effects of the extra tags on GPHR because GOLAC-2 was examined as an endogenous protein without manipulation, in addition to differences between the protein species, preparation methods and composition of buffer and liposomes. Taking these observations together, it is possible that GPHR is identical to GOLAC-2. □

## METHODS

**Establishment of mutant C27 cells.** CHO-derived 3B2A cells stably expressing the human DAF and CD59 GPI-anchored proteins were stably transfected with a combination of plasmids for an inducible reporter system (pTRE2pur-VSVGts<sup>ex</sup>-FF-mEGFP-GPI and pUHR62-1; gift from W. Hillen, Erlangen University, Erlangen, Germany). Cells expressing the reporter protein at high levels after incubation with Dox were sorted by a FACS Vantage (BD Biosciences) and cloned by limiting dilution. One clone was selected for further analysis and designated FF8. To establish cells exhibiting delayed transport of the reporter protein, FF8 cells were treated with 400 µg ml<sup>-1</sup> ethyl methanesulfonate for 24 h and cultured for one week. Next, cells with slowed surface expression of the reporter protein were enriched by several rounds of cell sorting using the FACS Vantage. Mutant cells defective in genes involved in biosynthesis and lipid remodelling of GPI (such as PIG-O and PGAP1) were also enriched as anticipated, and these cells were eliminated by cell sorting. The cell sorting was performed based on a transport assay, as described below, in the first, second, fourth and sixth rounds of cell sorting, normal surface expression of CD59 in the third round to eliminate cells defective in GPI-anchor biosynthesis, and PI-PLC sensitivity of CD59 in the fifth round to eliminate PGAP1-mutant cells. In the sixth round of cell sorting, the transport assay was carried out by transient transfection of pME-Neo2dH-VSVGts<sup>ex</sup>-FF-mEGFP-GPI using an electroporator (Bio-Rad) instead of induction of the endogenous reporter protein by Dox to eliminate cells that exhibited defective induction of the reporter system. The population obtained by this sorting procedure was subjected to limiting dilution and one clone was named the HR23-1C27 cell line (hereafter referred to as C27 cells).

**Transport assay of reporter proteins.** Cells derived from FF8 cells were cultured in complete medium containing 1 µg ml<sup>-1</sup> Dox at 40 °C for 24 h and quickly harvested with trypsin-EDTA solution (Sigma) followed by incubation in complete medium at 32 °C for the indicated times. The cells were stained with an M2 anti-Flag antibody and PE-conjugated goat anti-mouse Ig, and analysed using a FACSCalibur (BD Biosciences) or the FACS Vantage. In some cases, cells were transiently transfected with expression plasmids for reporter proteins using Lipofectamine 2000 (Invitrogen). At 10–12 h after transfection, the temperature was shifted to 40 °C and the cells were cultured for a further 24 h, followed by incubation at 32 °C for the indicated times. In addition to the first gating (FSC and SSC), a second gating to select cells expressing the same amount of reporter protein (brightness of EGFP in FL1) was performed for analysis using the CellQuest Pro software (BD).

**Immunoelectron microscopy.** Ultrathin cryosections were prepared as described previously<sup>43</sup>. The sections were rinsed with PBS containing 0.02 M glycine, blocked with 1% BSA in PBS and incubated with a mouse anti-HA antibody (1:10; Sigma) overnight at 4 °C. The sections were then incubated with goat anti-mouse or mouse IgG conjugated with 10 nm colloidal gold particles (GE Healthcare) for 1 h at room temperature, followed by fixation with 1% glutaraldehyde in PBS. After completion of the labelling, the sections were embedded in a thin layer of 2% methylcellulose containing 0.4% uranyl acetate (pH 4.0), air-dried and observed with a Hitachi H-7100 electron microscope. For control experiments, ultrathin sections were directly incubated with the secondary antibodies without pretreatment with the primary antibody.

**Measurement of Golgi and TGN pH.** C27+Vec and C27+GPHR cells plated on glass-bottomed dishes (Matsunami) the day before measurement of pH were analysed under a Fluoview FV1000 laser scanning confocal microscope (Olympus) equipped with an LD laser 405 (405 nm) and a multiline Ar laser (457, 488 and 515 nm) at room temperature. After preincubation of the cells in Na-Ringer buffer (140 mM NaCl, 2 mM CaCl<sub>2</sub>, 1 mM MgSO<sub>4</sub>, 1.5 mM K<sub>2</sub>HPO<sub>4</sub>, 10 mM glucose, 10 mM MES and 10 mM HEPES at pH 7.3) for 10 min, pFluorin-fused proteins were consecutively excited at wavelengths of 405 and 457 nm and the emitted fluorescence was captured through a spectral slit for wavelengths of 500–600 nm. More than 100 of regions of interest (ROIs) were automatically set with a threshold by MetaMorph 3.0 (Molecular Devices) in 12–16 cells expressing pFluorin-fused pH-sensor proteins (Fig. 4d). The emission intensities excited by 405 and 457 nm in the same ROI were measured by MetaMorph 3.0 using the region transfer and measurement functions. The data were imported into Microsoft Excel for calculation of the intensity ratios (405 nm:457 nm) and further analyses. For calibration curves, cells expressing each pFluorin-fused protein were incubated in calibration buffer (140 mM KCl, 2 mM CaCl<sub>2</sub>, 1 mM MgSO<sub>4</sub>, 1.5 mM K<sub>2</sub>HPO<sub>4</sub>, 10 mM glucose, 10 μM nigericin, 10 μM monensin, 10 mM MES and 10 mM HEPES) adjusted to various pHs (5.5, 6.0, 6.3, 6.6, 6.8, 7.1 or 7.5) for 10 min at room temperature for pre-equilibration and analysed as described above. For semi-intact cells, Na-Ringer buffer was replaced with permeabilization buffer (10 mM NaCl, 50 mM KCl, 90 mM K-gluconate, 2 mM CaCl<sub>2</sub>, 1 mM MgSO<sub>4</sub>, 2 mM K<sub>2</sub>HPO<sub>4</sub>, 4 mM EGTA and 20 mM HEPES at pH 7.25) supplemented with 0.5 μg ml<sup>-1</sup> streptolysin-O (Bio Academia) for 5 min and then with permeabilization buffer alone for 8 min to deplete intracellular ATP. Where indicated, 4 mM ATP was added back to the buffer to restore ATP-dependent V-ATPase activity. In each experiment, several cells were monitored at the same time and analysed by the MetaMorph software to calculate the pH.

**Planar-lipid bilayer.** A mixture of 3.2 mg egg phosphatidylcholine (Avanti Polar Lipids) and 0.8 mg bovine brain phosphatidylserine (Sigma) was dissolved in 0.4 ml chloroform, transferred to a glass test tube, dried under a gentle stream of nitrogen and centrifuged under high vacuum in a speed-vac (Tomy) for 1 h. For reconstitution of hGPHR-FHAT in liposomes, the lipid film (4 mg) was dissolved in 400 μl buffer (60 mM octyl-β-deoxyglucoside, 300 mM NaCl, 2 mM EDTA and 40 mM Tris-HCl at pH 7.4). Half of the lipid suspension (2 mg) was mixed with 450 μl of purified hGPHR-FHAT (~10 μg) and dialysed three times against 1 L of 100 mM KCl, 0.05% Na<sub>3</sub> and 10 mM HEPES-NaOH (pH 7.4) for 24 h. The recombinant proteins were incorporated into the lipid bilayers by vesicle fusion. Artificial lipid bilayers were formed as previously described<sup>44</sup>. Horizontal lipid bilayers of approximately 100 μm in diameter were prepared by painting a lipid solution (20 mg ml<sup>-1</sup> soybean lecithin in n-decane) across a plastic hole. Reconstituted liposomes were suspended in a hyperosmotic solution containing 300 mM sucrose, 150 mM KCl and 10 mM HEPES (pH 7.4), and a small amount of this suspension was added to the upper side of the lipid bilayer membrane. The liposomes spontaneously fused with the planar-lipid bilayer, resulting in incorporation of hGPHR-FHAT protein into the membrane. Currents across the membrane were recorded with a patch clamp amplifier (CEZ2400; Nihon Kohden). Membrane voltage was defined as the electrical potential of the upper compartment with reference to that of the bottom compartment held at virtual ground. The upper compartment (voltage command side) was connected to the head-stage input, and the bottom compartment was connected to the virtual ground using Ag-AgCl electrodes via an agar bridge containing 3 M KCl. Currents through the voltage-clamped bilayers were low-pass filtered at 10 kHz and recorded after digitization through an A/D converter (Digidata 1322A; Axon Instruments). Data were digitized at 1 kHz using pClamp9 software (Axon Instruments). Single-channel events were analysed using Clampfit9 software (Axon Instruments). Permeability ratios were determined using the Goldman-Hodgkin-Katz voltage equation.

*Note: Supplementary Information is available on the Nature Cell Biology website.*

#### ACKNOWLEDGMENTS

We thank F. Mori and K. Kinoshita for excellent technical assistance, and K. Nakamura for help with the cell sorting. We also thank T. Yoshimori, S. Kimura and H. Oomori for allowing us to use confocal and electron microscopes and for technical direction, and H. Hibino, H. Takeshima and T. Yamazaki for helpful discussions. This work was supported by grants from the Precursory Research for Embryonic Science and Technology, Japan Science and Technology Agency (Y.M.).

the Core Research for Evolutional Science and Technology, Japan Science and Technology Agency (T.K.) and the Ministry of Education, Culture, Sports, Science and Technology of Japan.

#### AUTHOR CONTRIBUTIONS

T.I. performed the planar lipid-bilayer analyses. M.K. and Y.U. performed the electron microscopy analyses. Y.M. performed the other experiments. T.K. and Y.M. contributed to the planning of experiments and wrote the manuscript. All authors discussed the results and commented on the manuscript.

#### COMPETING FINANCIAL INTERESTS

The authors declare no competing financial interests.

Published online at <http://www.nature.com/naturecellbiology/>  
Reprints and permissions information is available online at <http://npg.nature.com/reprintsandpermissions>

1. Weisz, O. A. Organelle acidification and disease. *Traffic* **4**, 57–64 (2003).
2. Tartakoff, A., Vassalli, P. & Detraz, M. Comparative studies of intracellular transport of secretory proteins. *J. Cell Biol.* **79**, 694–707 (1978).
3. Palokangas, H., Metsikko, K. & Vaananen, K. Active vacuolar H<sup>+</sup>-ATPase is required for both endocytic and exocytic processes during viral infection of BHK-21 cells. *J. Biol. Chem.* **269**, 17577–17585 (1994).
4. Presley, J. F., Mayor, S., McGraw, T. E., Dunn, K. W. & Maxfield, F. R. Bafilomycin A1 treatment retards transferrin receptor recycling more than bulk membrane recycling. *J. Biol. Chem.* **272**, 13929–13936 (1997).
5. Axelsson, M. A. *et al.* Neutralization of pH in the Golgi apparatus causes redistribution of glycosyltransferases and changes in the O-glycosylation of mucins. *Glycobiology* **11**, 633–644 (2001).
6. Rivinoja, A., Kokkonen, N., Kellokumpu, I. & Kellokumpu, S. Elevated Golgi pH in breast and colorectal cancer cells correlates with the expression of oncofetal carbohydrate T-antigen. *J. Cell. Physiol.* **208**, 167–174 (2006).
7. Puri, S., Bachert, C., Fimmel, C. J. & Linstedt, A. D. Cycling of early Golgi proteins via the cell surface and endosomes upon luminal pH disruption. *Traffic* **3**, 641–653 (2002).
8. Chapman, R. E. & Munro, S. Retrieval of TGN proteins from the cell surface requires endosomal acidification. *EMBO J.* **13**, 2305–2312 (1994).
9. Reaves, B. & Banting, G. Vacuolar ATPase inactivation blocks recycling to the trans-Golgi network from the plasma membrane. *FEBS Lett.* **345**, 61–66 (1994).
10. Kellokumpu, S., Sormunen, R. & Kellokumpu, I. Abnormal glycosylation and altered Golgi structure in colorectal cancer: dependence on intra-Golgi pH. *FEBS Lett.* **516**, 217–224 (2002).
11. Weisz, O. A. Acidification and protein traffic. *Int. Rev. Cytol.* **226**, 259–319 (2003).
12. Stobrawa, S. M. *et al.* Disruption of ClC-3, a chloride channel expressed on synaptic vesicles, leads to a loss of the hippocampus. *Neuron* **29**, 185–196 (2001).
13. Piwon, N., Gunther, W., Schwake, M., Bosl, M. R. & Jentsch, T. J. ClC-5 Cl<sup>-</sup>-channel disruption impairs endocytosis in a mouse model for Dent's disease. *Nature* **408**, 369–373 (2000).
14. Andresson, T., Sparkowski, J., Goldstein, D. J. & Schlegel, R. Vacuolar H<sup>+</sup>-ATPase mutants transform cells and define a binding site for the papillomavirus E5 oncoprotein. *J. Biol. Chem.* **270**, 6830–6837 (1995).
15. Moriyama, Y. & Nelson, N. H<sup>+</sup>-translocating ATPase in Golgi apparatus. Characterization as vacuolar H<sup>+</sup>-ATPase and its subunit structures. *J. Biol. Chem.* **264**, 18445–18450 (1989).
16. Glickman, J., Croen, K., Kelly, S. & Al-Awqati, Q. Golgi membranes contain an electrogenic H<sup>+</sup> pump in parallel to a chloride conductance. *J. Cell Biol.* **97**, 1303–1308 (1983).
17. Xie, X. S., Stone, D. K. & Racker, E. Determinants of clathrin-coated vesicle acidification. *J. Biol. Chem.* **258**, 14834–14838 (1983).
18. Hara-Chikuma, M. *et al.* ClC-3 chloride channels facilitate endosomal acidification and chloride accumulation. *J. Biol. Chem.* **280**, 1241–1247 (2005).
19. Grabe, M. & Oster, G. Regulation of organelle acidity. *J. Gen. Physiol.* **117**, 329–344 (2001).
20. Llopis, J., McCaffery, J. M., Miyawaki, A., Farquhar, M. G. & Tsien, R. Y. Measurement of cytosolic, mitochondrial, and Golgi pH in single living cells with green fluorescent proteins. *Proc. Natl. Acad. Sci. USA* **95**, 6803–6808 (1998).
21. Schapiro, F. B. & Grinstein, S. Determinants of the pH of the Golgi complex. *J. Biol. Chem.* **275**, 21025–21032 (2000).
22. Wu, M. M. *et al.* Organelle pH studies using targeted avidin and fluorescein-biotin. *Chem. Biol.* **7**, 197–209 (2000).
23. Wu, M. M. *et al.* Mechanisms of pH regulation in the regulated secretory pathway. *J. Biol. Chem.* **276**, 33027–33035 (2001).
24. Demaurex, N., Furuya, W., D'Souza, S., Bonifacino, J. S. & Grinstein, S. Mechanism of acidification of the trans-Golgi network (TGN). *In situ* measurements of pH using retrieval of TGN38 and furin from the cell surface. *J. Biol. Chem.* **273**, 2044–2051 (1998).
25. Nishi, T. & Forgac, M. The vacuolar H<sup>+</sup>-ATPases — nature's most versatile proton pumps. *Nature Rev. Mol. Cell Biol.* **3**, 94–103 (2002).
26. Pusch, M., Zifarelli, G., Murgia, A. R., Picollo, A. & Babini, E. Channel or transporter? The CLC saga continues. *Exp. Physiol.* **91**, 149–152 (2006).
27. Jentsch, T. J. Chloride and the endosomal-lysosomal pathway: emerging roles of CLC chloride transporters. *J. Physiol.* **578**, 633–640 (2007).

28. Duncan, R. R., Westwood, P. K., Boyd, A. & Ashley, R. H. Rat brain p64H1, expression of a new member of the p64 chloride channel protein family in endoplasmic reticulum. *J. Biol. Chem.* **272**, 23880–23886 (1997).
29. Nagasawa, M., Kanzaki, M., Iino, Y., Morishita, Y. & Kojima, I. Identification of a novel chloride channel expressed in the endoplasmic reticulum, golgi apparatus, and nucleus. *J. Biol. Chem.* **276**, 20413–20418 (2001).
30. Nordeen, M. H., Jones, S. M., Howell, K. E. & Caldwell, J. H. GOLAC: an endogenous anion channel of the Golgi complex. *Biophys. J.* **78**, 2918–2928 (2000).
31. Thompson, R. J., Nordeen, M. H., Howell, K. E. & Caldwell, J. H. A large-conductance anion channel of the Golgi complex. *Biophys. J.* **83**, 278–289 (2002).
32. Hara-Chikuma, M., Wang, Y., Guggino, S. E., Guggino, W. B. & Verkman, A. S. Impaired acidification in early endosomes of ClC-5 deficient proximal tubule. *Biochem. Biophys. Res. Commun.* **329**, 941–946 (2005).
33. Miesenbock, G., De Angelis, D. A. & Rothman, J. E. Visualizing secretion and synaptic transmission with pH-sensitive green fluorescent proteins. *Nature* **394**, 192–195 (1998).
34. Kim, J. H. *et al.* Dynamic measurement of the pH of the Golgi complex in living cells using retrograde transport of the verotoxin receptor. *J. Cell Biol.* **134**, 1387–1399 (1996).
35. Farinas, J. & Verkman, A. S. Receptor-mediated targeting of fluorescent probes in living cells. *J. Biol. Chem.* **274**, 7603–7606 (1999).
36. Yamashiro, D. J. & Maxfield, F. R. Acidification of morphologically distinct endosomes in mutant and wild-type Chinese hamster ovary cells. *J. Cell Biol.* **105**, 2723–2733 (1987).
37. Paroutis, P., Touret, N. & Grinstein, S. The pH of the secretory pathway: measurement, determinants, and regulation. *Physiology* **19**, 207–215 (2004).
38. Johnson, L. S., Dunn, K. W., Pytowski, B. & McGraw, T. E. Endosome acidification and receptor trafficking: baflomycin A1 slows receptor externalization by a mechanism involving the receptor's internalization motif. *Mol. Biol. Cell* **4**, 1251–1266 (1993).
39. Laver, D. R. & Peter, W. G. Interpretation of substrates in ion channels: unipoles or multipores? *Prog. Biophys. Mol. Biol.* **67**, 99–140 (1997).
40. Scheel, O., Zdebik, A. A., Lourdell, S. & Jentsch, T. J. Voltage-dependent electrogenic chloride/proton exchange by endosomal CLC proteins. *Nature* **436**, 424–427 (2005).
41. Graves, A. R., Curran, P. K., Smith, C. L. & Mindell, J. A. The Cl<sup>-</sup>/H<sup>+</sup> antiporter CLC-7 is the primary chloride permeation pathway in lysosomes. *Nature* **453**, 788–792 (2008).
42. Wright, E. M. & Diamond, J. M. Anion selectivity in biological systems. *Physiol Rev.* **57**, 109–156 (1977).
43. Koike, M. *et al.* Cathepsin D deficiency induces lysosomal storage with ceroid lipofuscin in mouse CNS neurons. *J. Neurosci.* **20**, 6898–6906 (2000).
44. Ide, T. & Yanagida, T. An artificial lipid bilayer formed on an agarose-coated glass for simultaneous electrical and optical measurement of single ion channels. *Biochem. Biophys. Res. Commun.* **265**, 595–599 (1999).

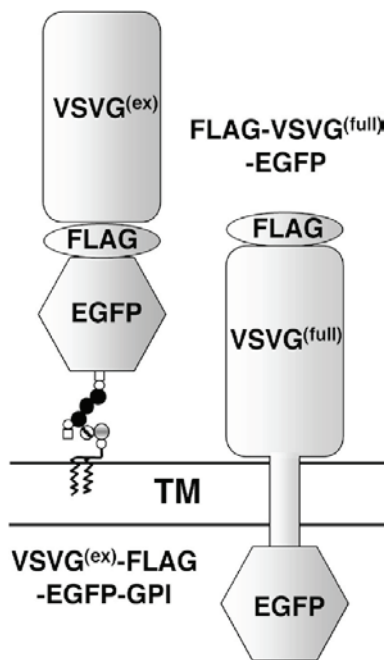


**Figure S1** Schematic diagrams of reporter proteins. VSVG<sup>(ex)</sup>-FLAG-EGFP-GPI is composed of an extracellular domain of temperature-sensitive vesicular stomatitis virus G protein (VSVG<sup>(ex)</sup>), a furin cleavage sequence (not shown), a FLAG-tag, green fluorescent protein (EGFP) and a

glycosylphosphatidylinositol (GPI)-attachment signal sequence derived from CD59. FLAG-VSVG<sup>(full)</sup>-EGFP is composed of a FLAG-tag, full-length temperature-sensitive VSVG (VSVG<sup>(full)</sup>) and green fluorescent protein (EGFP). TM: transmembrane domain.

## SUPPLEMENTARY INFORMATION

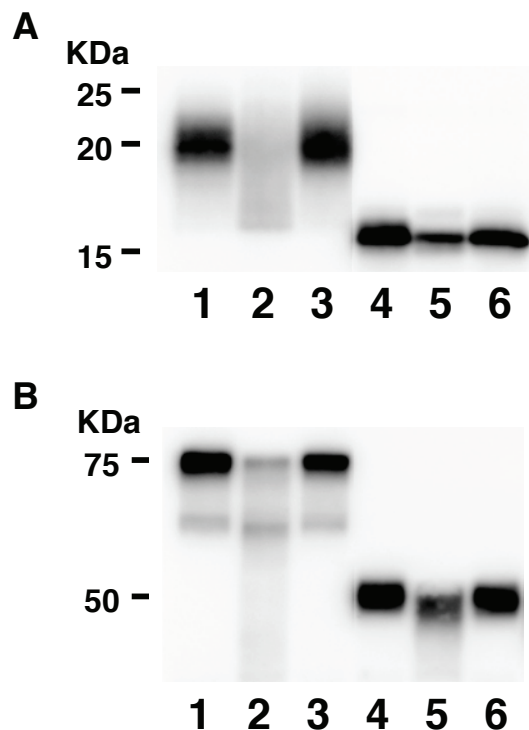


**Figure S2** SDS-PAGE analysis of CD59 treated with N-glycanase and DAF treated with sialidase. **(A)** FLAG-tagged CD59 expressed in FF8 (lanes 1 and 4), C27 (lanes 2 and 5) and GPHR-transfected C27 (lanes 3 and 6) cells was incubated in the absence (lanes 1-3) or presence (lanes 4-6) of N-glycanase and analyzed by SDS-PAGE and western blotting with an

antibody against CD59. **(B)** FLAG-tagged DAF-N95S, which lacked the sole N-glycosylation site due to mutagenesis, expressed in FF8 (lanes 1 and 4), C27 (lanes 2 and 5) and GPHR-transfected C27 (lanes 3 and 6) cells was incubated in the absence (lanes 1-3) or presence (lanes 4-6) of sialidase and analyzed by SDS-PAGE and western blotting with an antibody against DAF.

|             |     |  |
|-------------|-----|--|
| Human       | 1   | -----MSFLIDSSIMITSQILFFFGFWLFFMRQLFKDYEIRQYVVQVIFSVDFAFSCTMFEL   |
| Mouse       | 1   | -----MSFLIDSSIMITSQILFFFGFWLFFMRQLFKDYEVRQYVVQVIFSVDFAFSCTMFEL   |
| Hamster     | 1   | -----MSFLIDSSIMITSQILFFFGFWLFFMRQLFKDYEVRQYVVQVIFSVDFAFSCTMFEL   |
| Dog         | 1   | -----MSFLIDSSIMITSQILFFFGFWLFFMRQLFKDYEVRQYVVQVIFSVDFAFSCTMFEL   |
| Xenopus     | 1   | -----MSFADSVLMVISQQLFFFGFWLFFMRQLFKDYEVRQYVVQVIFSVDFAFSCTMFEL  |
| Drosophila  | 1   | -----MIFFAGGWLFVNKELFKHYEIRHISVQLIFSSTFALSIITMFEL  |
| Arabidopsis | 1   | MGYGWGIGFEGLMLVIGSLCLLGSAGLWFLNRRLYKEYEERKALVQIIFSVVFAFSCNLQL  |
| Human       | 58  | IIFEILGVLNSSSSRYFHWMNLCVILLILVF MVPFYIGYFIVSNIRLLHKQRL-LFSCLL  |
| Mouse       | 58  | IIFEILGVLNSSSSRYFHWMNLCVILLILVF MVPFYIGYFIVSNIQLLHKQRL-LFSCLL  |
| Hamster     | 58  | IIFEILGVLNSSSSRYFHWMNLCVILLILVF MVPFYIGYFIVSNIQLLHKQRL-LFSCLL  |
| Dog         | 58  | IIFEILKVLNSSSSRYFHWMNLCVILLILVF MVPFYIGYFIVSNIRLLHKQRL-LFSCLL  |
| Xenopus     | 58  | IIFEILKVLNSSSSRYFHWMNLCVILLVLVFVVPFYIGYFVVSNIQLLHKRQL-LFSCCL   |
| Drosophila  | 44  | IIFEIIVDVLLESSSSRYFHWRGLTLLFMTTAVIPIVICYSVIHSISFFSDKWVRLTTFC   |
| Arabidopsis | 61  | VLFEEIPVVLSEARMVNWVKVDFCLIVLLVFMLPVYHCYLMLRNTGVRRERAAG-VGALLF  |
| Human       | 117 | WLTFMYFFWKLGDPFPILSPKHGILSIEQLISRGVVIGVTLMALLSGFGAVNCPTYMSY  |
| Mouse       | 117 | WLTFMYFFWKLGDPFPILSPKHGILSIEQLISRGVVIGVTLMALLSGFGAVNCPTYMSY  |
| Hamster     | 117 | WLTFMYFFWKLGDPFPILSPKHGILSIEQLISRGVVIGVTLMALLSGFGAVNCPTYMSY  |
| Dog         | 117 | WLTFMYFFWKLGDPFPILSPKHGILSIEQLISRGVVIGVTLMALLSGFGAVNCPTYMSY  |
| Xenopus     | 117 | WLTFMYFFWKLGDPFPILSPKHGILSIEQLISRGVVIGVTLMALLSGFGAVNCPTYMSY  |
| Drosophila  | 104 | WFIFIYGLWRIGDPFPILSASHGIFTIEQGVSLRIVIGVTMAILSGFGAVNYPYTSMSY  |
| Arabidopsis | 120 | LTAFLYAFWRMGTHFPMPDS-DKGFFSMPQLVSRIGVIGVTLMAVLSGFGAVNLPYSYSL   |
| Human       | 177 | FRLRNVTDTDILALERLLQTMDMIISKKRMAARRTMFQKGEVHNKPSG-----FWGM  |
| Mouse       | 177 | FRLRNVTDTDILALERLLQTMDMIISKKRMAVARRTMFQRGDVQNKPSSG-----LWGM  |
| Hamster     | 177 | FRLRNVTDTDILALERLLQTMDMIISKKRMAVARRTMFQRGEVQNKPSSG-----LWGM  |
| Dog         | 177 | FRLRNVTDADIVALERLLQTMDMIISKKRMAARRTMFQKGEVHNKPSG-----FWGM  |
| Xenopus     | 177 | FRLRNVTDADIALERLLQTMDMIISKKRMAARRTMFQKGEVHNKPSG-----FWGM   |
| Drosophila  | 164 | FIKPVSRNDIICFERRLAATVEMLSAKKRKIAAMAIYNHNKLNP--SKPRI-----WDML   |
| Arabidopsis | 179 | FIREIEESEIKSLERQLMQSMETCIAKKKKILLCQVEVERSLVSEEHQKGKSFFRREVGT   |
| Human       | 231 | IKSVTTSASGSENLTLIQQEVDALEELSRQLFLETADLYATKERIEYSKTFKGKYFNFLG   |
| Mouse       | 231 | LKSVTASAPGSENLTLIQQEVDALEELSRQLFLETADLYATKERIEYSKTFKGKYFNFLG   |
| Hamster     | 231 | LKSVTASAPGSENLTLIQQEVDALEELSRQLFLETADLYATKERIEYSKTFKGKYFNFLG   |
| Dog         | 231 | IKSVTTSAPGSENLTLIQQEVDALEELSRQLFLETADLYATKERIEYSKTFKGKYFNFLG   |
| Xenopus     | 231 | IKSVTTSAPVSENLTYQIQQEVDALEELSRQLFLETADLHATKERIEYSKTFQGKYFNFLG  |
| Drosophila  | 216 | ASAVQRNTNSGEDINQLKQEVYGLEELRSVFLSLLKNMEERQRWSOTLKGKYFNFLG  |
| Arabidopsis | 239 | VVRCSVQDDQKEQDIKLMEAeveGLEELSKQLFLEYLRQAKDAAFSRTWKGHVQNFLG   |
| Human       | 291 | YFFSIYCVWKIFMATINIVFDRVKGKDPVTRGIEITVNYLGIQFDVKFWSQHISFILVGI   |
| Mouse       | 291 | YFFSIYCVWKIFMATINIVLDRVKGKDPVTRGIEITVNYLGIQFDVKFWSQHISFILVGI   |
| Hamster     | 291 | YFFSIYCVWKIFMATINIVLDRVKGKDPVTRGIEITVNYLGIQFDVKFWSQHISFILVGI   |
| Dog         | 291 | YFFSIYCVWKIFMATINIVFDRVKGKDPVTRGIEITVNYLGIQFDVKFWSQHISFILVGI   |
| Xenopus     | 291 | YFFSIYCVWKIFMATINIVFDRVKGKDPVTRGIEITVNYLGIQFDVKFWSQHISFILVGI   |
| Drosophila  | 276 | HFFS <del>V</del> YCVYKIFMCCINIIFDRVGRKD <del>P</del> VTRGIEIAIHWC <del>G</del> FNIDFAFWNQHISF <del>L</del> VGC                  |
| Arabidopsis | 299 | YACSIYCVYKMLKSLSQSVVFKEAGTKDPVTMMISIFLQFFD <del>I</del> GVDAALLSQVISLLFIGM   |
| Human       | 351 | IIVTSIRGLLITLT <del>K</del> FFYAISSSKSSNVIVVLLAQIMGMYFVSSVLLIRMSMP <del>EYRT</del>   |
| Mouse       | 351 | IIVTSIRGLLITLT <del>K</del> FFYAISSSKSSNVIVVLLAQIMGMYFVSSVLLIRMSMP <del>EYRT</del>   |
| Hamster     | 351 | IIV <del>S</del> IRGLLITLT <del>K</del> FFYAISSSKSSNVIVVLLAQIMGMYFVSSVLLIRMSMP <del>EYRT</del>                                   |
| Dog         | 351 | IIVTSIRGLLITLT <del>K</del> FFYAISSSKSSNVIVVLLAQIMGMYFVSSVLLIRMSMP <del>EYRT</del>   |
| Xenopus     | 351 | IIVTSIRGLLITLT <del>K</del> FFYAISSSKSSNVIVVLLAQIMGMYFVSSVLLIRMSMP <del>EYRT</del>   |
| Drosophila  | 336 | IIVTSIRGLLITLT <del>K</del> FFYRISSSKSSNVIVVLLAQIMGMYFVSSVLLIRMSMP <del>EYRT</del>   |
| Arabidopsis | 359 | LIVISVRGFLTNLMKFFF <del>A</del> VS <del>R</del> VGSG <del>S</del> SSNVVLFLSEIMGMYFLSS <del>T</del> LLIRKSLRNEYRG                 |
| Human       | 409 | IITEV <del>L</del> G-ELOFNFYHRWF <del>D</del> VIFLV <del>S</del> ALSS <del>S</del> ILFLYLAHKQAPEKOMAP-                           |
| Mouse       | 409 | IITEV <del>L</del> G-ELQFNFYHRWF <del>D</del> VIFLV <del>S</del> ALSS <del>S</del> ILFLYLAHKQAPEKHM <del>AP</del> -              |
| Hamster     | 409 | IIT <del>Q</del> V <del>L</del> G-ELQFNFYHRWF <del>D</del> VIFLV <del>S</del> ALSS <del>S</del> ILFLYLAHKQAPEKHM <del>AP</del> - |
| Dog         | 409 | IITEV <del>L</del> G-ELQFNFYHRWF <del>D</del> VIFLV <del>S</del> ALSS <del>S</del> ILFLYLAHKQAPEKHM <del>AP</del> -              |
| Xenopus     | 409 | IITEV <del>L</del> G-ELOFNFYHRWF <del>D</del> VIFLV <del>S</del> ALSS <del>S</del> ILFLYLAHKQAPEKHM <del>AL</del> -              |
| Drosophila  | 394 | IITEV <del>L</del> G-NL <del>H</del> FNFYHRWF <del>D</del> VIFLV <del>S</del> ALTTIIVLYLSRKPV <del>R</del> VDDSDLN               |
| Arabidopsis | 419 | IITDV <del>L</del> GGDIO <del>F</del> YHRWF <del>D</del> AIFVASAFLS <del>L</del> LLSAHY <del>T</del> SRQIDKHPID                  |

**Figure S3** Alignment of human GPHR protein sequence with homologues of other species. Human GPHR (XP\_001133516) was aligned with mouse (NP\_080505), hamster (AB362891), dog (XP\_540275), xenopus (NP\_001086744), drosophila (NP\_611016) and arabidopsis

(NP\_001031235) homologues using software of ClastalW and BoxShade. Protein sequence identities to human GPHR are 96% (mouse), 96% (hamster), 98% (dog), 92% (xenopus), 56% (drosophila) and 42% (arabidopsis).

## SUPPLEMENTARY INFORMATION

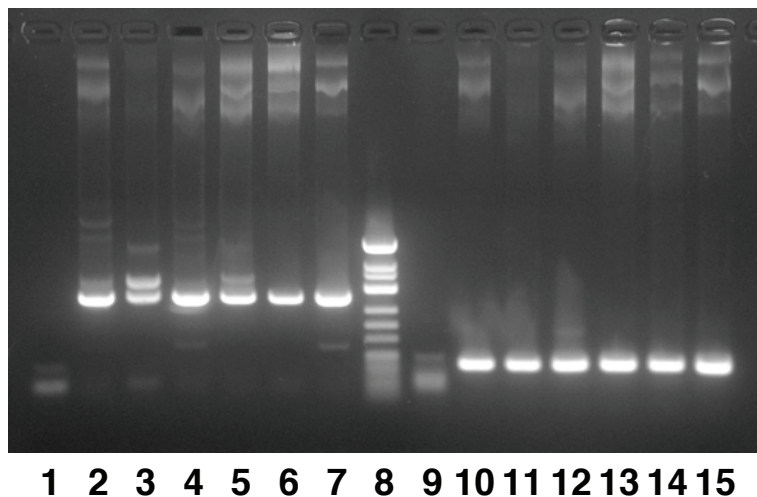


**Figure S4a** GPHR transcripts were efficiently amplified by PCR in all six cDNA libraries (derived from human brain tissues, placental tissues, HeLa cells, Hep3B cells, KT3 cells and CHO cells) examined . No cDNA (lanes 1 and 9), human brain (lanes 2 and 10), HeLa (lanes 3 and 11), Hep3B (lanes 4 and 12), KT3 (lanes 5 and 13), human placenta (lanes

6 and 14) and another HeLa (lanes 7 and 15) cDNA libraries were used for PCR with two primer sets (F1: 5'-CCCATACACTTACATGTCTTACTT and R1: 5'-AATTAAAATTTCCCCTTGAAGGT, lanes 1 - 7) and F2: 5'-GATCGAGTTGGGAAAACGG and R2: 5'-GAAGGAAATGTGTTGGGACC, lanes 9 - 15). Lane 8: molecular markers.

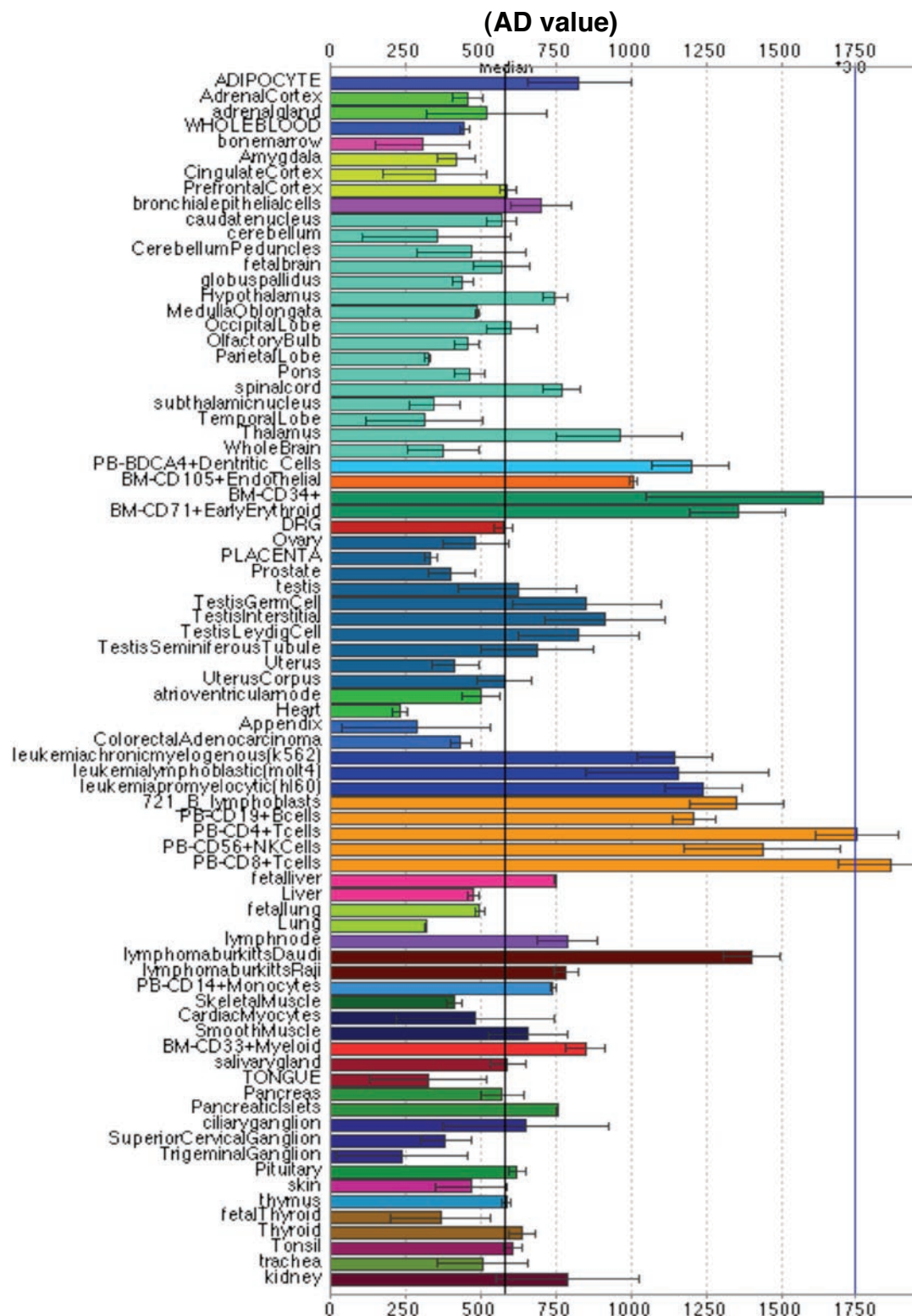


**Figure S4b** The expression profile of human GPHR transcript in various tissues. The data is taken from <http://symatlas.gnf.org/SymAtlas/>. The human GNF1H gene chip and MAS5 algorithm were used for the analysis of

GPHR transcript. An average difference (AD) value of 200 was defined as a conservative threshold to call a gene expressed, which indicated that GPHR was expressed in all 79 tissues examined.

## SUPPLEMENTARY INFORMATION

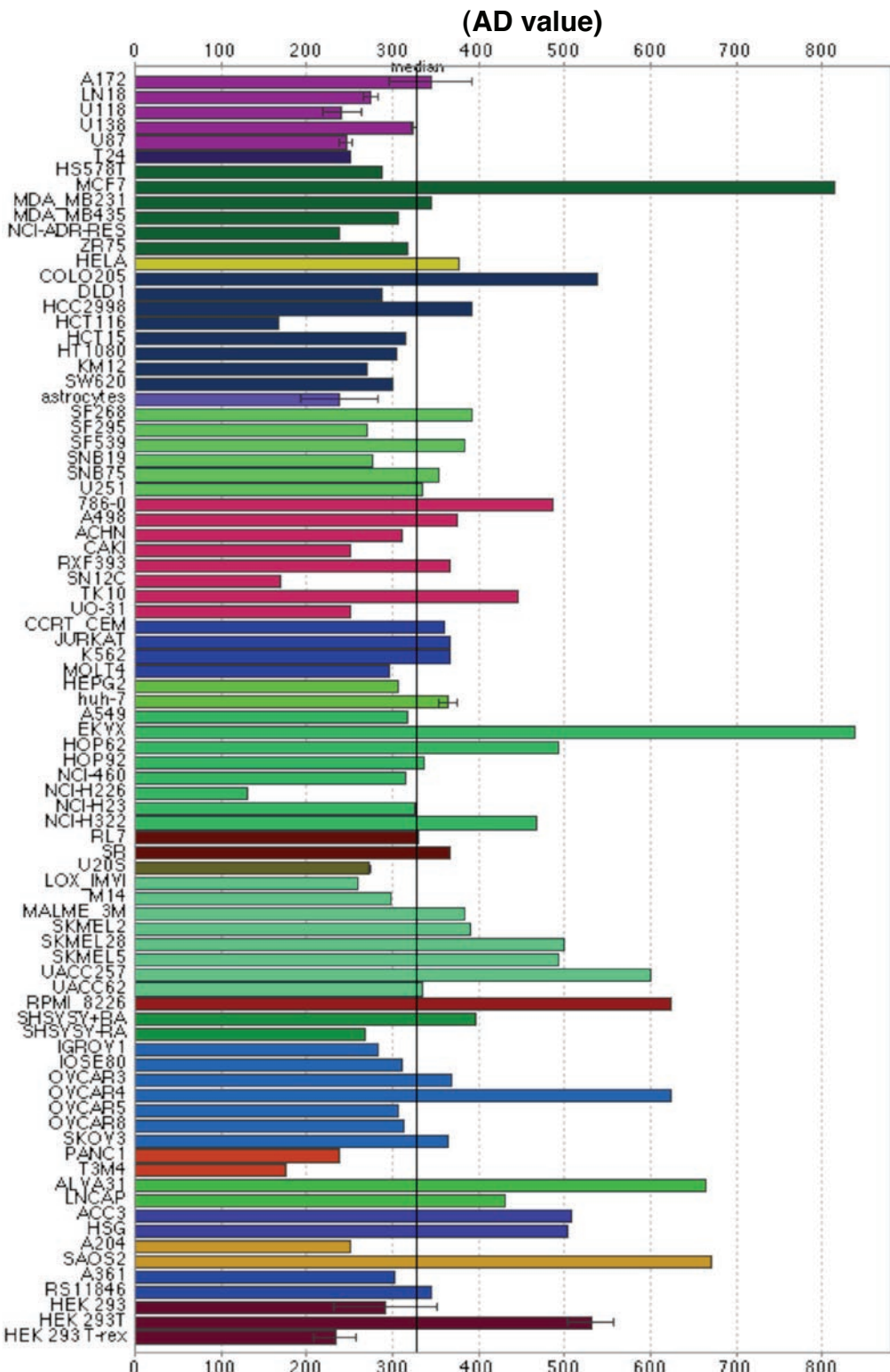


**Figure S4c** The expression profile of human GPHR transcript in various cell lines. The data is taken from <http://symatlas.gnf.org/SymAtlas/>. The human U133A gene chip and MAS5 algorithm were used for the analysis of

GPHR transcript. An average difference (AD) value of 200 was defined as a conservative threshold to call a gene expressed, which indicated that GPHR was expressed in 80 of 84 cell lines (4 were just below the positive criteria).

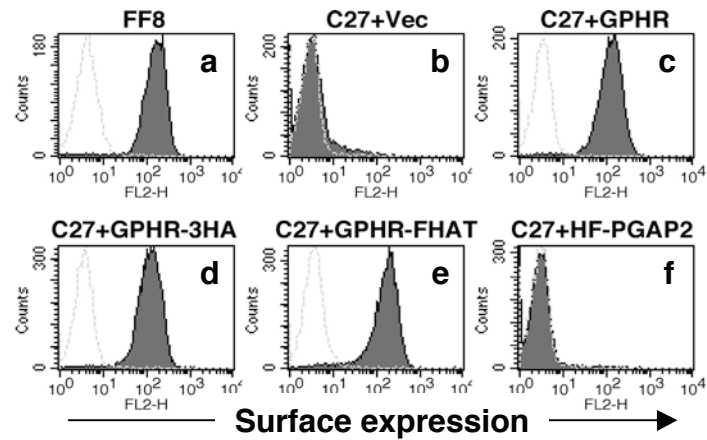


**Figure S5** GPHR tagged with 3HA or FHAT is functional. (a to f) Transport assays of the VSVG<sup>(ex)</sup>-FLAG-EGFP-GPI reporter protein were performed in parent FF8 cells (a), C27+Vec cells (b), C27+GPHR cells (c), C27+GPHR-3HA cells (d), C27+GPHR-FHAT cells (e) and C27+HF-PGAP2 cells as a

negative control (f). All cell lines, except for FF8, are stable cell lines in which C27 mutant cells are permanently transfected with the indicated expression plasmids. Surface expression of the reporter protein was assessed by staining at 45 min after the temperature shift to 32°C.

## SUPPLEMENTARY INFORMATION

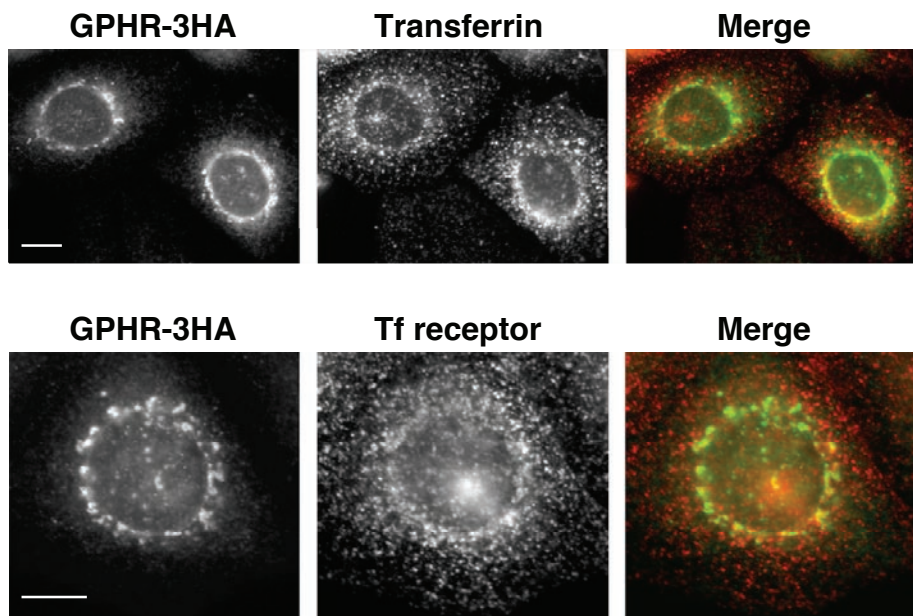


**Figure S6** GPHR is not colocalized with endosomal proteins. GPHR-3HA (left panels), transferrin endocytosed for 1 h (upper middle) and transferrin (Tf) receptor (lower middle) were stained in C27 cells stably expressing functional GPHR-3HA. Bars indicate 10  $\mu$ m.

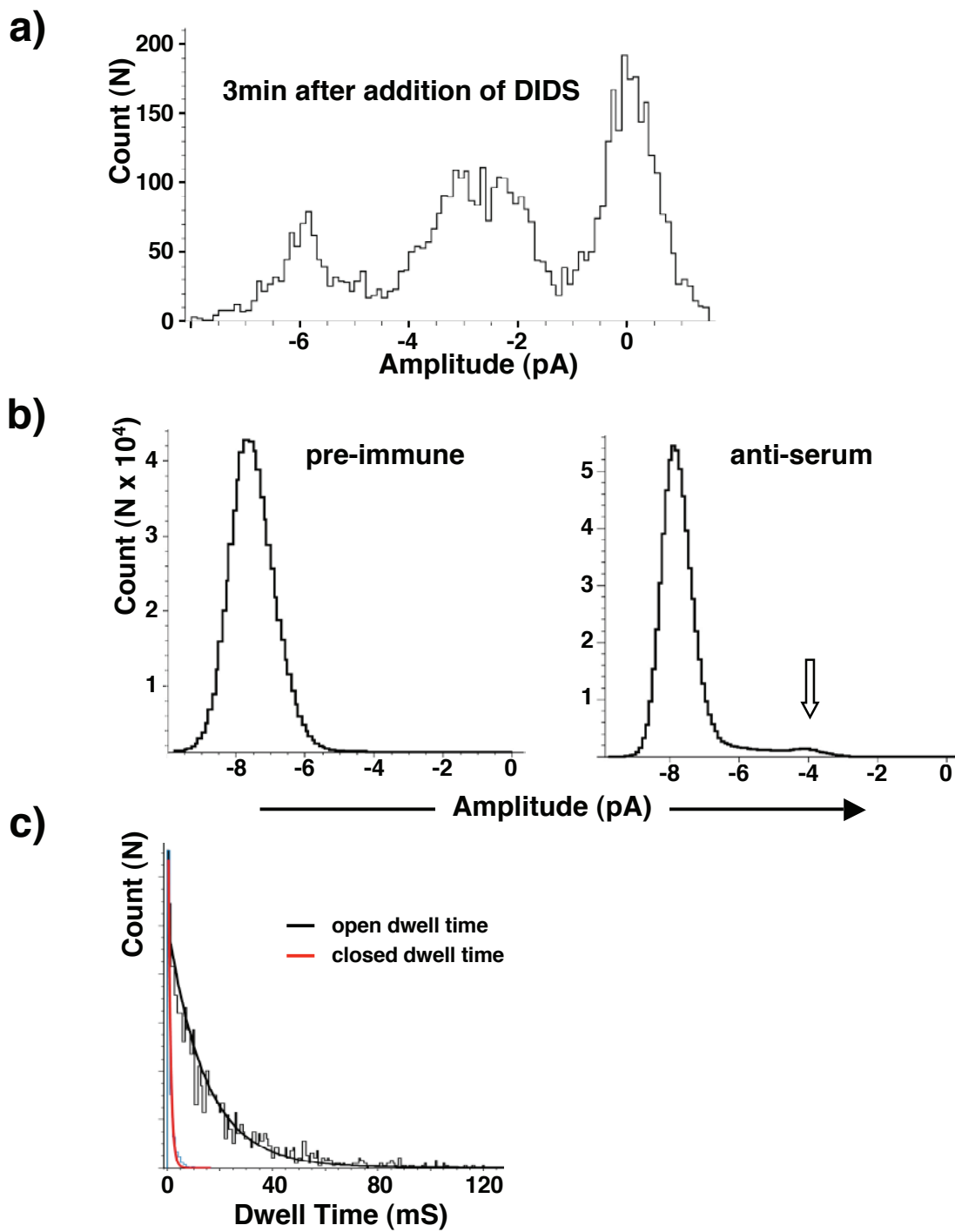


**Figure S7** Effects of DIDS and anti-serum on GPHR channel activity. (a) Amplitude histogram generated at a holding potential of  $-10\text{ mV}$  and 3 min after addition of 1 mM DIDS as described in figure 5, (e). (b) Amplitude histogram generated at a holding potential of  $-10\text{ mV}$  after addition of pre-immune serum (left) and anti-serum (right) as described in figure 5, (f). About 5% of points was indicated as closed state (arrow) in the presence of anti-serum whereas almost

no closed state was observed in pre-immune serum. (c) Dwell time histogram generated after addition of anti-serum as described in (b). Open dwell time distribution was fit by a single exponential and estimated mean open time was 14 mS (black line), whereas the open and closed dwell times in the presence of pre-immune serum were not estimated since the channel opened constitutively and the open probability was almost 1.0 as described in (b).

## SUPPLEMENTARY INFORMATION

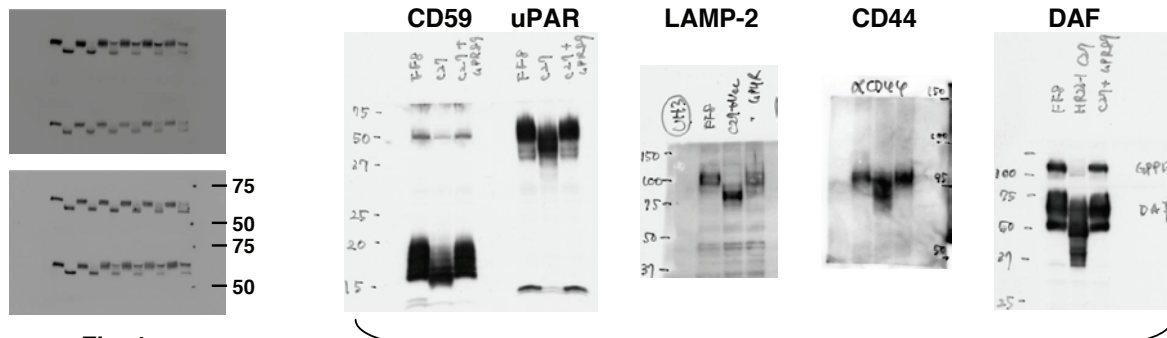


**Fig. 1c**  
(CCD camera)

**Fig. 2a**

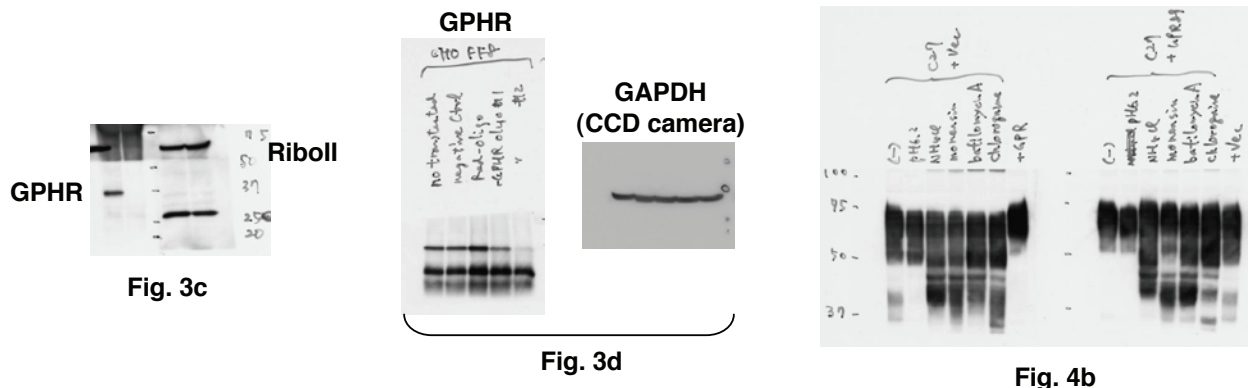


**Fig. 3c**

**Fig. 3d**

**Fig. 4b**

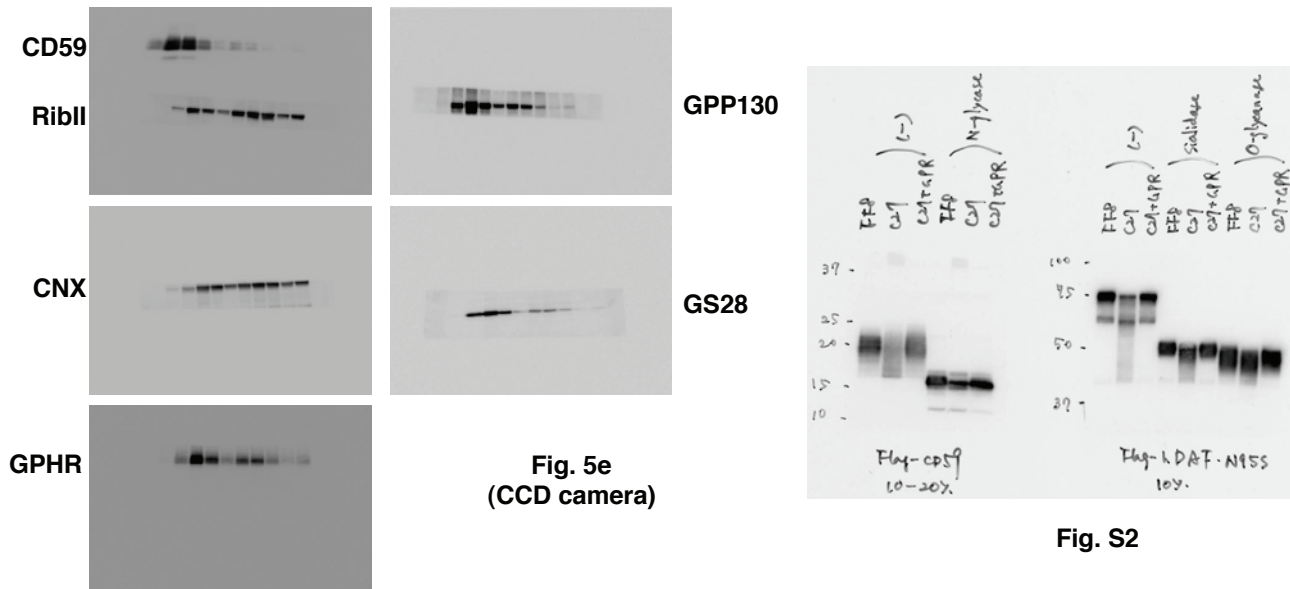


**Fig. 5e**  
(CCD camera)

**Fig. S2**

**Figure S8** Full scans of the Western blots from the figures indicated.

## Supplementary Information

### MATERIALS and METHODS

#### Cell culture and establishment of the mutant C27 cell line and its derivative cells

All cell lines used in this paper were derivatives of Chinese hamster ovary (CHO) cells. Cell lines were cultured in Ham's F12 medium (Sigma) supplemented with 10% fetal calf serum (FCS). Various combinations of 600 µg/ml G418, 6 µg/ml puromycin, 600 µg/ml hygromycin, 6 µg/ml blasticidin and 200 µg/ml zeocin were added to the medium for maintenance of the transfected plasmids. 3B2A cells were described previously<sup>1</sup>. pUHrT 62-1 was a gift from Dr. W. Hillen (Erlangen University)<sup>2</sup>. To establish retrovirus infection-competent C27 cells, mouse CAT1, a receptor for ecotropic retroviruses, was stably expressed by transfection of pME-hyg-mCAT1 (a gift from Dr. K. Ohishi, Osaka University) and a clone obtained by limiting dilution under hygromycin selection was termed C27mCAT1-1. C27+Vec, C27+GPHR, C27+GPHR-3HA and C27+GPHR-FHAT cells were established from C27mCAT1-1 cells by infection with retroviruses produced in PLAT-E packaging cells (a gift from Dr. T. Kitamura, University of Tokyo) transfected with pLIB2-pgkBSD, pLIB2-hGPHR-pgkBSD, pLIB2-hGPHR-3HA-pgkBSD and pLIB2-hGPHR-FHAT-pgkBSD, respectively, followed by selection with blasticidin. To establish pH-sensor cells, C27+Vec and C27+GPHR cells were stably transfected with pME-zeo-pHluorin-TGN38, pME-zeo-GPP130-pHluorin or pME-zeo-GnTI-pHluorin under selection with zeocin.

The delayed protein transport in C27+Vec cells was obvious for both GPI-anchored and transmembrane cargos, but was more prominent for the GPI-anchored reporter protein. This finding may be due to the construction or nature of this reporter, since efficient surface expression of the protein depended on the presence of a furin cleavage sequence between VSVG<sup>(ex)</sup> and a FLAG-tag. Site-directed mutagenesis of the consensus sequence for furin cleavage prominently weakened the surface expression, and the intact reporter protein expressed on the cell surface lacked the VSVG<sup>(ex)</sup> portion, since it was detected by an anti-FLAG antibody but hardly by an anti-VSVG<sup>(ex)</sup> (8G5F11) antibody (data not shown). Since furin is localized in the TGN and acidic conditions are critical for its activation<sup>3</sup>, and since the acidic pH in the TGN was significantly elevated in C27 mutant cells (see below), the difference in the transport rates of the two reporter proteins in C27 cells may be explained by inefficient cleavage of the GPI-anchored reporter protein.

#### Plasmids

We generated pME-Neo2dH-VSVGts<sup>(ex)</sup>-FF-mEGFP-GPI for expression of a GPI-anchored form of the reporter protein, termed VSVGts<sup>(ex)</sup>-FLAG-EGFP-GPI, which

was composed of the extracellular domain of temperature-sensitive vesicular stomatitis virus G protein (amino acids 1-464 of VSVGtsO45), a linker (GDHPPKGGGSGGGSGGGSVD), a furin cleavage sequence (SRHRSKR), a FLAG-tag, mutated green fluorescent protein (EGFP) bearing a mutation of leucine 221 to lysine to reduce homotypic binding and the GPI-attachment signal from CD59 (ENGGTSLSEKTVLLLVTPLAAWSLHP). The plasmid also contained a neomycin-resistance gene. We generated pME-FLAG-VSVG<sup>(full)</sup>-EGFP for expression of a transmembrane form of the reporter protein by replacing the CD59 portion of pME-FLAG-CD59 with a cDNA for VSVG-EGFP (a gift from Dr. V. Malhotra, University of California, San Diego) lacking the N-terminal 16-amino-acid signal sequence. pTRE2pur-VSVGts<sup>(ex)</sup>-FF-mEGFP-GPI was constructed by excising VSVGts<sup>(ex)</sup>-FF-mEGFP-GPI from pME-Neo2dH-VSVGts<sup>(ex)</sup>-FF-mEGFP-GPI and inserting it into the pTRE2pur vector (Clontech). pLIB2-pgkBSD was constructed by subcloning pgk-BSD, which expresses a blasticidin-resistance gene under the control of the pgk promoter, into the pLIB retrovirus vector (Clontech). The human GPHR fragment excised by SfiI from pLIB-hGPHR (clon6) was subcloned into the same site in pLIB2-pgkBSD, producing pLIB2-hGPHR-pgkBSD. In pLIB2-hGPHR-3HA-pgkBSD and pLIB2-hGPHR-FHAT-pgkBSD, hGPHR was fused with three tandem HA tags or FLAG-HAT tandem tags at the C-terminus. The pME-pHluorin-tag plasmid was constructed by subcloning ratiometric pHluorin amplified by PCR from pGEX-pHluorin (a gift from Dr. G. Miesenboeck, Yale University and Dr. J. Rothman, Columbia University) into the pME vector. To construct pME-zeo-GPP130-pHluorin and pME-zeo-GnTI-pHluorin plasmids, amino acids 1-107 of rat GPP130 and 1-99 of human N-acetylglucosaminyltransferase I were fused with the N-terminus of pHluorin, respectively, and subcloned into pME-zeo, which contains a zeocin-resistance gene. To construct pME-zeo-pHluorin-TGN38, the C-terminal 56 amino acids of rat TGN38 were fused with the C-terminus of pHluorin, and subcloned into the pME-zeo vector.

### Antibodies and materials

The antibodies used were mouse monoclonal antibodies against GM130 (BD Biosciences), EEA1 (BD Biosciences), FLAG-tag (clone M2; Sigma), HA-tag (clone HA7; Sigma), VSVG-tag (clone P5D4; Roche), GS28 (StressGen), ribophorin I (Santa Cruz Biotechnology), transferrin receptor (Zymed), lamp2 (clone UH3; Developmental Studies Hybridoma Bank at the University of Iowa) and GM3 (a gift from Dr. K. Furukawa, Nagoya University), rat monoclonal antibodies against CD44 (BD Biosciences), rabbit polyclonal antibodies against GPP130 (Covance), calnexin (Stressgene), HA-tag (MBL), transferrin (Biomedica) and GRASP65 (a gift from Drs. C. Sutterlin and V. Malhotra, University of California, San Diego) and a goat polyclonal antibody against ribophorin II (Santa Cruz Biotechnology). Mouse monoclonal antibodies

against CD59, DAF and uPAR were described in a previous paper<sup>4</sup>. Mouse monoclonal and rabbit polyclonal antibodies against GPHR were developed as follows. A PCR fragment corresponding to amino acids 170-287 of human GPHR was amplified with the primers hGPR89-F1 (5'-ccacggatcCCCATACACTTACATGTCTTACTT-3') and hGPR89-R1 (5'-gcaggtcgactAATTAAAATATTCCCCCTGAAGGT-3') and subcloned into the BamHI-SalI site of the pQE80L vector (Qiagen). The plasmid was transformed with XL10-Gold (Stratagene) and used for production of His-tagged recombinant partial GPHR. The recombinant protein was purified by Ni-NTA resin (Qiagen) and used to immunize mice and rabbits several times. Mouse hybridoma cells (clones 31-5 (IgG1, *k*) and 25-5 (IgG2a, *k*)) and a rabbit antiserum were obtained in standard ways. The secondary antibodies used were horseradish peroxidase (HRP)-conjugated anti-mouse IgG, anti-rabbit IgG (Amersham Biosciences) and anti-goat IgG (Promega), PE-conjugated goat anti-mouse IgG (PharMingen) and streptavidin (Biomeda) and Alexa 488-conjugated goat anti-mouse IgG and Alexa 594-conjugated goat anti-rabbit IgG (Molecular Probes). FITC-conjugated peanut agglutinin (PNA) and biotin-conjugated GS-II were purchased from Seikagaku Co. and Molecular Probes, respectively.

### PI-PLC treatment

Samples containing 1-2 x 10<sup>6</sup> cells were incubated in 50 µl of F-12 medium containing 0.1% BSA, 0.5 mM EDTA and 50 mU PI-PLC (Invitrogen; final concentration, 1 U/ml) at 37°C for 1 h.

### Cloning of human and CHO GPHRs

C27mCAT1-1 cells were infected with a human brain retroviral cDNA library (Clontech). After transport assays at 32°C for 1 h (see above), the cells were stained with the M2 anti-FLAG antibody and goat anti-mouse IgG magnetic microbeads (Miltenyi Biotec), and cells expressing high levels of the reporter protein were enriched twice by Auto-MACS (Miltenyi Biotec). Several cell lines that exhibited normal transport of the reporter protein were obtained by limiting dilution from the enriched cell pool. Genomic DNAs were extracted from each cell line, and retrovirus-derived cDNAs integrated into the genome were amplified by PCR with 5'-XhoI (5'-TGTCTCGAGCCCTCACTCCTCTCTAG-3') and 3'-NotI (5'-TTGCGGCCGCACCTACAGGTGGGGTCTT-3') primers. The obtained PCR products were digested with SfiI and subcloned into the same sites of the pLIB vector (Clontech). Next, retroviruses were produced and infected into C27mCAT1-1 cells to examine whether the obtained cDNAs restored the delayed transport in the transport assays. Two human GPHR clones (C6 and C8) were finally obtained and sequenced. The hamster GPHR cDNA was amplified from a CHO cDNA library by PCR using the degenerate primers dF1 (5'-TTTGGNNTYGGNTGGYTNTTYTTYATG-3') and dR1 (5'-

GCCATNTGYTTYTCNGGNGCYTG-3'). Based on the sequence obtained from the PCR product, we designed four internal primers, F1 (5'-GTACTTCGTCTCTTCCGTGCTG-3'), F2 (5'-GTGCCCTCTCCAGCATACTGTTC-3'), R1 (5'-AGGAAGTAGGACATGTATGTGTACGG-3') and R2 (5'-CAGGCCACAGGAGACAGGAAAAGA-3'). The remaining 5' and 3' regions were amplified from the CHO cDNA library by nested PCR using combinations of R1, R2 and two vector-specific primers for the 5' region and combinations of F1, F2 and two vector-specific primers for the 3' region, respectively. The complete sequence obtained for hamster GPHR was submitted to the GenBank database (Accession number, AB362891). Hamster GPHR was amplified by RT-PCR from C27mCAT1-1cells with F0 (5'-CCTTCCCTGAGGTGTAGACAGC-3') and R0 (5'-GCCCTGGTACAGGTACTACCCAT-3') primers, and the sequence was verified using a 3100 Avant sequencer (Applied Biosystems).

### **Knockdown of GPHR by RNA interference**

Oligonucleotides for RNA interference (*Silencer* Select predesigned siRNA products) were purchased from Ambion (catalogue numbers: oligonucleotide #1, s168367; oligonucleotide #2, s168369; negative control oligonucleotide, 4390843). A final concentration of 24 µM of each oligonucleotide was transfected using Lipofectamine RNAiMAX (Invitrogen) according to the manufacturer's instructions. For transport assays and measurement of Golgi pH, wild-type FF8 cells were transfected with the oligonucleotides twice with an interval of about 60 h. The amounts of endogenous GPHR were analyzed by immunoprecipitation followed by Western blotting as described in the section entitled "Subcellular fractionation".

### **In silico analyses**

The programs used for in silico analyses are listed below.

SOSUI: <http://sosui.proteome.bio.tuat.ac.jp/sosuiframe0E.html>

BLAST:

[http://www.ncbi.nlm.nih.gov/BLAST/Blast.cgi?CMD=Web&PAGE\\_TYPE=BlastHome](http://www.ncbi.nlm.nih.gov/BLAST/Blast.cgi?CMD=Web&PAGE_TYPE=BlastHome)

GNF SymAtlas: <http://symatlas.gnf.org/SymAtlas/>

### **Immunofluorescence microscopy**

Cells were washed with PBS, fixed with PBS containing 4% paraformaldehyde for 20 min at room temperature, permeabilized with PBS containing 1% BSA, 0.1% NaN<sub>3</sub> and 0.1% TX-100, and stained with combinations of primary antibodies and Alexa 488- or 594-conjugated goat secondary antibodies. In the case of UH3 anti-lamp2, 0.1% saponin was used instead of TX-100 for permeabilization. Images of the stained cells were acquired using a BX50 microscope equipped with a 100x/1.35 UPlanApo oil immersion

objective (Olympus) and a VB-6010 charge-coupled device (CCD) camera (Keyence).

### **Subcellular fractionation**

Approximately  $3 \times 10^8$  wild-type FF8 cells were washed with PBS, suspended in 4 ml of homogenization buffer (0.25 M sucrose and 10 mM HEPES-KOH, pH 7.2) containing a cocktail of protease inhibitors without EDTA (Roche) and homogenized by nitrogen cavitation (150 psi for 15 min) followed by 15 strokes of a tight Dounce homogenizer. The cell lysate was centrifuged at 780 g for 10 min and the supernatant was recovered. The pellet was suspended in 1.5 ml of homogenization buffer, passed through a 24-gauge needle ten times and homogenized by 10 strokes of a tight Dounce homogenizer. After centrifugation at 2,000 g for 5 min, the second supernatant was combined with the first supernatant and centrifuged again at 2,000 g for 10 min. The resulting supernatant was added to homogenization buffer to a final volume of 11 ml with 100  $\mu$ l of a 1.8-M sucrose cushion at the bottom, and ultracentrifuged at 288,000 g for 1 h. The pellet corresponding to the membrane fraction was suspended in 3 ml of homogenization buffer. An aliquot (1.5 ml) of the membrane suspension was loaded on top of a discontinuous sucrose gradient consisting of 2.5 ml of 1.6 M, 1.5 ml of 1.4 M, 4 ml of 1.2 M and 2 ml of 0.7 M sucrose containing 10 mM HEPES-KOH (pH 7.2) from the bottom, and ultracentrifuged at 200,000 g for 18 h. Subsequently, 1-ml fractions were removed from the top by a Piston Gradient Fractionator (Biocomp). Aliquots of each fraction were separated by SDS-PAGE using a 4-20% gradient gel and analyzed by Western blotting with antibodies against organelle marker proteins. The intensities of the positive bands were quantified using a CCD luminescent image analyzer (Fujifilm). For quantification of endogenous GPHR, each 1-ml fraction was diluted with 4 ml of 10 mM Hepes-KOH (pH 7.2) and ultracentrifuged at 200,000 g for 1 h. The pellets were suspended in 0.8 ml of lysis buffer (1% TX-100, 150 mM NaCl, 1 mM EDTA and 20 mM Tris-HCl, pH 7.4) containing a cocktail of protease inhibitors, incubated on ice for 30 min and centrifuged at 20,000 g for 10 min. The supernatants were incubated with 4  $\mu$ l of a rabbit antiserum against GPHR overnight followed by incubation with 35  $\mu$ l of a 50% slurry of protein G Sepharose (GE Healthcare) for 5 h. The protein G beads were washed four times with 0.8 ml of lysis buffer, and incubated with 40  $\mu$ l of sample buffer on ice for 10 min. An aliquot (25  $\mu$ l) of each eluate was separated by SDS-PAGE, subjected to Western blotting with mouse monoclonal antibody C31-5 against GPHR and evaluated as described above.

### **Immunoelectron microscopy using ultrathin cryosections**

Ultrathin cryosections were prepared as described<sup>5</sup>. Briefly, cells were fixed with 4% paraformaldehyde in with 0.1 M phosphate buffer (pH 7.2; PB) for 24 h at 4°C, collected, washed with PBS containing 0.02 M glycine and embedded in 12% gelatin in 0.1 M PB. Small blocks of the gelatin-embedded samples were rotated in 2.3 M sucrose in 0.1 M PB

overnight at 4°C. The blocks were then placed in a specimen holder (Leica) and quickly plunged into liquid nitrogen. Ultrathin cryosections (60 nm) were cut with a Leica UC6/FC6 at approximately -120°C using a cryoP diamond knife (Diatome), picked up with a 1:1 mixture of 2% methylcellulose and 2.3 M sucrose in 0.1 M PB<sup>6</sup> and transferred to nickel grids carrying a carbon-coated Formvar supporting film.

**Electron microscopy.** Cells cultured on Celldesk (Sumitomo Bakelite) were fixed with 2% glutaraldehyde and 2% paraformaldehyde in 0.1 M phosphate buffer (pH 7.2; PB), post-fixed with 1% OsO<sub>4</sub> in 0.1 M PB, block-stained with a 2% aqueous solution of uranyl acetate, dehydrated through a graded series of ethanol and embedded in Epon 812. Ultrathin sections were cut with an ultramicrotome (Ultracut N; Reichert-Nissei), stained with uranyl acetate and lead citrate, and observed with a Hitachi H7100 electron microscope.

#### **Quantitative analysis of the labelling density**

Sections of cells with or without immunolabelled Golgi areas were photographed and printed at a final magnification of  $\times 42,000$ . The number of cells analyzed was 33. The compartments evaluated were as follows: Golgi apparatus (G); peri-Golgi vesicles (V); endosomes or lysosomes (E/L); endoplasmic reticulum (ER); outer nuclear membrane (N); outer mitochondria membrane (M); and plasma membrane (P). The peri-Golgi vesicles were arbitrarily defined as vesicles that were circular, about 70 nm in diameter and located around the Golgi cisternae but not connected or continuous with them. The linear density was quantified by scanning electron micrographs and measuring the lengths of the linear profiles of various membranes with an electronic pen (Wacom) using ImageJ software version 1.38x for Macintosh (NIH). The numbers of gold particles on the cross-sectional membrane profiles within 30 nm from the center of the membrane were counted as positive signals, and the labelling densities were expressed as the number of gold particles per unit membrane length ( $\mu\text{m}$ ). The data represent the mean values obtained from the 33 different cells  $\pm$  s.e.m. Data were analyzed by one-way ANOVA followed by the Tukey-Kramer *post hoc* test.

#### **Measurement of lysosomal pH**

For measurement of lysosomal pH, FF8, C27+Vec and C27+GPHR cells were incubated in serum-free medium supplemented with 0.2 mg/ml of fluorescein- and tetramethylrhodamine-double-labelled dextran (MW: 70 kDa; Molecular Probes) for 24 h, washed twice with PBS and incubated in prewarmed FCS-containing medium for a further 4 h. The cells were then harvested and suspended in phenol red-free DMEM supplemented with 5% FCS and 20 mM HEPES (pH ~7.3) at room temperature. For calibration curves, FF8 cells were suspended in calibration buffers (140 mM NaCl, 2 mM

CaCl<sub>2</sub>, 1 mM MgSO<sub>4</sub>, 1.5 mM K<sub>2</sub>HPO<sub>4</sub>, 10 mM glucose, 4 µM nigericin, 4 µM monensin and either 20 mM succinic acid (pH 5, 5.5 and 6) or 10 mM MES/10 mM HEPES (pH 6.5 and 7)) for 10 min at room temperature for pre-equilibration. The cells were analyzed using a FACSCalibur equipped with a 488-nm Ar laser. Emitted fluorescence was captured through a 530/30 band pass filter (FL1) for fluorescein and a 630/22 band pass filter (FL3) for tetramethylrhodamine in a linear mode. The ratios of the intensities (FL3/FL1) from 30,000 cells were calculated using FlowJo (Digital Biology). Statistical analysis was performed according to Student's *t*-test using JMP software (SAS Institute Inc.).

### **Recycling assay of transferrin (Tf)**

Lysosomal pHs in FF8 (lane 1), C27+Vec (lane 2) and C27+GPHR (lane 3) cells were calculated by the ratio of the fluorescence intensity of tetramethylrhodamine to that of fluorescein by FACS after endocytosis of fluorescein- and tetramethylrhodamine-double-labelled dextran. FF8, C27+Vec and C27+GPHR cells were incubated in complete DMEM supplemented with 15 µg/ml human Tf for 90 min, washed four times with cold PBS containing 0.5% BSA and harvested with trypsin/EDTA. After neutralization of the trypsin with soybean trypsin inhibitor (Sigma), the cells were centrifuged into a pellet and incubated in prewarmed FCS-free DMEM containing 0.5% BSA at 37°C for the indicated time periods. After one wash with PBS, the cells were lysed. The whole cell lysates were separated by SDS-PAGE using a 7.5% gel and analyzed by Western blotting with anti-Tf and anti-ribophorin I antibodies. The intensities of the bands were quantified using a CCD luminescent image analyzer (Fujifilm) and the intensities of Tf were normalized by those of ribophorin I.

### **Transport assay of VSV-G protein with endoglycosidase-H**

C27+Vec and C27+GPHR cells were transfected with a temperature-sensitive VSVG expression plasmid (pME-VSVGts) using Lipofectamine 2000 and the temperature was shifted to 40°C at 10-12 h after transfection. After 24 h of incubation at 40°C, the cells were quickly harvested with trypsin-EDTA solution followed by incubation in complete medium containing 100 µg/ml cycloheximide at 32°C for the indicated time periods. Next, the cells were washed once with cold PBS, solubilized with lysis buffer (1% TX-100, 150 mM NaCl, 1 mM EDTA and 20 mM Tris-HCl, pH 7.4) containing a cocktail of protease inhibitors on ice for 30 min and centrifuged at 20,000 g for 10 min. Aliquots (9 µl) of the supernatants were mixed with 1 µl of 10x denaturing buffer (final concentrations of 1% SDS and 80 mM DTT), incubated at 100°C for 10 min and treated with endoglycosidase-H (NEB) overnight at 37°C. The reaction solutions were separated by SDS-PAGE using a 7.5% gel and VSVGts was detected with an anti-VSVG-tag antibody.

### **Production of recombinant GPHR-FHAT protein**

The pFastBac1-hGPHR-FHAT plasmid was constructed by subcloning hGPHR-FHAT into the SalI-XbaI sites of the pFastBac1 baculovirus expression vector (Invitrogen) and transfected into DH10Bac competent cells (Invitrogen). Baculovirus virions were produced according to the manufacturer's protocol and infected into Sf9 cells. An Sf9 cell pellet sample of about 5 g was lysed in 80 ml of buffer A (1% TX-100, 300 mM NaCl, 2 mM EDTA and 40 mM Tris-HCl, pH 7.4) containing a cocktail of protease inhibitors (Roche) for 1 h in a cold room. After sequential centrifugation of the lysate at 18,800 g for 10 min and 141,000 g for 1 h, the supernatant was applied to a column containing a 0.5-ml bed volume of M2 anti-FLAG beads (Sigma). The column was washed three times with 2 ml of buffer A and three times with 2 ml of buffer B (60 mM octyl- $\beta$ -deoxyglucoside, 300 mM NaCl and 40 mM Tris-HCl, pH 8.0). The bound proteins were eluted with 5 ml of buffer B containing 1 mg/ml of FLAG peptide (Sigma) and the eluate was incubated with 200  $\mu$ l of a 50% slurry of Ni-NTA resin overnight in a cold room. The Ni-NTA resin was washed four times with 1 ml of buffer B and the bound proteins were eluted with 450  $\mu$ l of buffer B containing 300 mM imidazole. The total amount of eluted hGPHR-FHAT was estimated to be about 10  $\mu$ g by comparison with BSA as a standard.

### **Measurement of the Golgi buffer capacity**

C27+Vec and C27+GPHR cells expressing GnTI-pHluorin were loaded with Na-Ringer buffer supplemented with 30 mM NH<sub>4</sub>Cl for 4 min. The buffer was then replaced with Na-Ringer buffer supplemented with 1  $\mu$ M bafilomycin. The pHs were monitored as described in the section entitled "Measurement of Golgi/TGN pH". The buffer capacity ( $\beta$ ) was calculated using the following equation:  $\beta = ([\text{NH}_4\text{Cl}]/\Delta\text{pH}) \cdot 10^{\{\text{pH}(\text{out}) - \text{pH}(\text{final})\}}$ , where  $\Delta\text{pH}$  and pH(final) are the pH increase and Golgi/TGN pH just after NH<sub>4</sub>Cl addition, respectively, and pH(out) is the perfusate pH<sup>7</sup>.

### **Analysis of GPHR protein complexes**

Approximately  $2 \times 10^8$  C27+hGPHR-FHAT cells were washed once with PBS and lysed in 14 ml of lysis buffer (1% digitonin, 150 mM NaCl, 1 mM EDTA and 20 mM Tris-HCl, pH 7.4) containing a cocktail of protease inhibitors for 1 h on ice. After centrifugation at 12,000 rpm for 10 min to remove insoluble materials, the supernatant was collected. GPHR-FHAT complexes were purified from the supernatant by sequential purification using M2 anti-FLAG beads and Ni-NTA resin as described in the section entitled "Production of recombinant GPHR-FHAT protein". The affinity-purified proteins were separated by blue-native gel electrophoresis (BN-PAGE; Invitrogen) according to the manufacturer's instructions. The proteins were then transferred to a PVDF membrane and analyzed by Western blotting with an antibody against the FLAG-tag to confirm that the

major band contained GPHR-FHAT. Alternatively, the major band stained with G-250 was excised from the gel and separated by SDS-PAGE, before the proteins were visualized by silver staining.

1. Tashima, Y. *et al.* PGAP2 is essential for correct processing and stable expression of GPI-anchored proteins. *Mol. Biol. Cell* **17**, 1410-1420 (2006).
2. Urlinger, S. *et al.* Exploring the sequence space for tetracycline-dependent transcriptional activators: novel mutations yield expanded range and sensitivity. *Proc. Natl. Acad. Sci. USA* **97**, 7963-7968 (2000).
3. Anderson, E.D., VanSlyke, J.K., Thulin, C.D., Jean, F. & Thomas, G. Activation of the furin endoprotease is a multiple-step process: requirements for acidification and internal propeptide cleavage. *Embo J* **16**, 1508-1518 (1997).
4. Maeda, Y. *et al.* Fatty acid remodeling of GPI-anchored proteins is required for their raft association. *Mol. Biol. Cell* **18**, 1497-1506 (2007).
5. Koike, M. *et al.* Cathepsin D deficiency induces lysosomal storage with ceroid lipofuscin in mouse CNS neurons. *J. Neurosci.* **20**, 6898-6906 (2000).
6. Liou, W., Geuze, H.J. & Slot, J.W. Improving structural integrity of cryosections for immunogold labeling. *Histochem. Cell Biol.* **106**, 41-58 (1996).
7. Sonawane, N.D. & Verkman, A.S. Determinants of [Cl<sup>-</sup>] in recycling and late endosomes and Golgi complex measured using fluorescent ligands. *J. Cell Biol.* **160**, 1129-1138 (2003).